Climate Modeling Through Radiative-Convective Models

V. RAMANATHAN AND J. A. COAKLEY, JR.

National Center for Atmospheric Research, Boulder, Colorado 80307

We present a review of the radiative-convective models that have been used in studies pertaining to the earth's climate. After familiarizing the reader with the theoretical background, modeling methodology, and techniques for solving the radiative transfer equation the review focuses on the published model studies concerning global climate and global climate change. Radiative-convective models compute the globally and seasonally averaged surface and atmospheric temperatures. The computed temperatures are in good agreement with the observed temperatures. The models include the important climatic feedback mechanism between surface temperature and H_2O amount in the atmosphere. The principal weakness of the current models is their inability to simulate the feedback mechanism between surface temperature and cloud cover. It is shown that the value of the critical lapse rate adopted in radiative-convective models for convective adjustment is significantly larger than the observed globally averaged tropospheric lapse rate. The review also summarizes radiative-convective model results for the sensitivity of surface temperature to perturbations in (1) the concentrations of the major and minor optically active trace constituents, (2) aerosols, and (3) cloud amount. A simple analytical model is presented to demonstrate how the surface temperature in a radiative-convective model responds to perturbations.

CONTENTS

Introduction and scope of the review 465
Fundamental concepts 465
Background 466
Modeling principles 466
Convective adjustment 467
Models for planetary and stellar atmospheres 467
Evaluation of solar and long-wave radiative fluxes 468
Absorption and emission of long-wave radiation 468
Absorption and scattering of solar radiation 469
Transmission for inhomogeneous optical paths 470
Miscellaneous details 471
Solving for the equilibrium temperature profile 472
Time-stepping method 472
Newton-Raphson method 472
Models for the earth's climate 473
External variables 473
Feedback mechanisms 474
Model studies of present climate 475
Present climate 475
Thermal structure 475
Radiative heating and cooling 476
Curtis-Godson and line shape approximations in calculations of stratospheric cooling rates 476
Sensitivity of the model surface temperature 478
Feedback mechanisms 480
Role of H_2O, CO_2, O_3, and clouds 481
Studies of climate change 482
Increase in CO_2 482
Increase in aerosols 483
Perturbations in O_3 and NO_2 484
Stratospheric H_2O 486
Minor trace species 486
Concluding Remarks 487

A. INTRODUCTION AND SCOPE OF THE REVIEW

This review describes the role of radiative-convective models in the theory of climate and climate change. One of the basic objectives of climate models is to determine qualitatively and quantitatively the various interactions and feedback mechanisms between the four basic components of the climate system, i.e., the surface, the hydrosphere, the atmosphere, and the cryosphere. The mutual coupling between these four climatic components gives rise to a myriad of interactive feedback processes, so many that as yet no single model has been able to incorporate all of these processes.

Paper number 8R0533.
0034-6853/78/048R-0533$06.00

In order to cope with this complex problem, climate modelers have taken the logical first step of developing models that incorporate a limited number of interactive processes. This approach has given rise to a hierarchy of models based on the number of dimensions, i.e., latitude, longitude, and altitude, included in the models. A very comprehensive review of the existing climate models and the model hierarchy has been given by *Schneider and Dickinson* [1974].

The simplest in the model hierarchy is the one-dimensional model. There are two categories of one-dimensional models. The first category is the surface energy balance model. Latitude is the only dimension considered in this model. The second category is the vertical column energy balance model. The radiative-convective model, the subject of this review, belongs to this category.

Altitude is the only dimension considered in the radiative-convective model. The model computes the vertical distribution of one of the basic variables that we associate with climate, i.e., the globally and annually averaged surface and atmospheric temperatures. In spite of its simplicity the radiative-convective model has provided valuable insights into problems of climate theory and climate change. Because of its simplicity, however, the model has limited applicability to the real climate system. We will attempt to present a balanced view of both the usefulness and the limited applicability of the model. After introducing the fundamental concepts and computational techniques employed in the model, our review will focus on the numerous climate experiments that have been performed with the aid of radiative-convective models.

Radiative-convective models have also been used extensively in studies concerned with stellar and planetary atmospheres. It is beyond the scope of this review to discuss these studies in detail. Nevertheless, we will cite some of the planetary and stellar atmosphere applications where they are applicable.

B. FUNDAMENTAL CONCEPTS

We will first define the symbols that will be used here.

z altitude;
t time;
T atmospheric temperature;
T_s surface temperature;

T_e equilibrium temperature of the planet;
q_S net solar radiative flux;
q_T net long-wave radiative flux;
Q net radiative heating, equal to $-(1/\rho c_p)[(dq_S/dz) + (dq_T/dz)]$;
ρ atmospheric density;
c_p specific heat at constant pressure;
g acceleration due to gravity;
R gas constant;
σ Stefan-Boltzmann constant, equal to 5.67×10^{-8} W m^{-2} °K^{-4}.

We will clarify the terminology used here for denoting the radiative energy emitted (and absorbed) by the surface and atmosphere. At temperatures characteristic of the earth's surface and atmosphere, most of the energy (roughly 99.8%) emitted by the earth-atmosphere system is contained at wavelengths greater than 4 μm. In meteorological and geophysical literature this radiation is alternatively referred to by one of the following names: infrared, long-wave, terrestrial, or thermal radiation. We will use the names thermal and long-wave radiation in this review.

1. Background

Traditionally, the starting point in the study of the thermal structure of the atmosphere, be it the earth's atmosphere or other planetary atmospheres, is the computation of the vertical temperature distribution within the atmosphere by assuming the entire surface-atmosphere system to be in radiative equilibrium. A comparison of the radiative equilibrium temperatures with the observed temperatures has indicated the extent to which other atmospheric processes, such as convection, large-scale circulation, and condensation processes, influence the thermal energy balance of the system. In most planetary atmospheres, radiative equilibrium temperatures cannot be sustained in the lower regions of the atmosphere. In the lower regions the vertical gradient of the radiative equilibrium temperature, dT/dz ($-dT/dz$ is known as the lapse rate), is negative and so steep that the gradient of potential temperature, $d\theta/dz$, is negative. A negative potential temperature gradient is unstable to convection [*Eliassen and Kleinschmidt,* 1957] and hence would lead to the onset of thermal (also known as natural or free) convection. Convection aids radiation in transporting energy from the surface of the planet to the atmosphere. The vertical transport of heat by convection tends to minimize the magnitude of $d\theta/dz$.

The radiative equilibrium temperature lapse rate depends, among other factors, on the optical depth of the atmosphere in the spectral region of the thermal radiation. This dependence on optical depth can be easily shown for a hypothetical atmosphere in which the absorption coefficient is independent of wavelength. Such an atmosphere is referred to as a gray atmosphere. For a gray atmosphere in radiative equilibrium the long-wave radiative flux is approximately given by [*Ambartsumyan,* 1958, p. 22]

$$q_T = \frac{4\sigma}{3}\frac{dT^4}{d\tau} \qquad d\tau = -K\rho\, dz \tag{1}$$

where τ is the optical depth, K the absorption coefficient, and ρ the density. The optical depth is measured from the top of the atmosphere; i.e., $\tau = 0$ at $z = \infty$. For simplicity of presentation the absorption of solar radiation by the atmosphere has been neglected. As a result the long-wave radiative flux q_T is required to be a positive constant in order to satisfy the condition of radiative equilibrium. If we assume hydrostatic equilibrium so that $\tau = KP/g$, where P is the pressure, we can solve (1) to obtain

$$\frac{-dT}{dz} = \frac{g}{4R}\frac{q_T\tau}{q_T\tau + c_1} \tag{2}$$

where c_1 is a constant to be determined from boundary conditions. We immediately note from (2) that $-dT/dz$ increases with τ and $dT/dz \to 0$ as $\tau \to 0$. In the atmosphere the optical depth generally decreases exponentially with increasing altitude, and hence $dT/dz \to 0$ for large values of z.

From the preceding discussions we can intuitively expect that in general there will be two regions in the atmosphere. The first to be discussed is the lower region in which the radiative equilibrium lapse rate is sufficiently steep to be unstable to convection. As was mentioned earlier, the criterion for instability is determined from the sign of $d\theta/dz$. The gradients of θ and T are related by

$$\frac{d\theta}{dz} = \frac{\theta}{T}\left(\frac{dT}{dz} + \frac{g}{c_p}\right) \tag{3}$$

The atmosphere is unstable when

$$d\theta/dz < 0 \tag{4}$$

i.e., when

$$-dT/dz > \Gamma \tag{5}$$

where $\Gamma = g/c_p$ is the adiabatic temperature gradient. When the lapse rate ($-dT/dz$) is greater than Γ, the atmosphere is called superadiabatic, while the converse situation is called subadiabatic. It has been assumed that an atmosphere with an initial superadiabatic radiative equilibrium lapse rate attains a final 'state of convective equilibrium' [*Chandrasekhar,* 1957]. The state of convective equilibrium as originally defined by Lord Kelvin is discussed in detail by *Chandrasekhar* [1957]. For our purpose it suffices to note that for convective equilibrium, $d\theta/dz = 0$. Physically, convective equilibrium implies that the convection mechanically stirs the atmosphere until a uniform potential temperature is maintained. We will return to the validity of this argument later.

The second region to be discussed is the overlying region which corresponds to the region in which the radiative equilibrium lapse rate is subadiabatic. If this region is not subjected to other energy transfer processes, it can remain in the state of radiative equilibrium. The situation described here has led to the concept of radiative-convective equilibrium models. According to *Chandrasekhar* [1957, p. 84] the concept of convective equilibrium was first introduced by Lord Kelvin in1862 to explain the gradient of temperature in the earth's lower atmosphere. The instability criterion for the radiative equilibrium temperature gradient (see (5)) was introduced by Schwarzschild (as was mentioned by *Chandrasekhar* [1957, p. 224]). In planetary atmospheres the lower region in which the radiative equilibrium lapse rate is superadiabatic is known as the troposphere, while the overlying region is known as the stratosphere, and the common boundary between these two regions is referred to as the tropopause.

2. Modeling Principles

The underlying principles and assumptions in the model formulation are best explained from consideration of the thermodynamic energy equation, given by

$$\frac{\partial}{\partial t}\rho c_p T + \nabla\cdot\rho c_p \mathbf{V}T + \frac{\partial}{\partial z}\rho c_p WT + \rho g W = Q + Q_F \tag{6}$$

where $\mathbf{V}$ is the horizontal velocity vector, W is the vertical velocity, and Q_F is the frictional heating. It should be noted that Q_F is present in (6) only when some of Q goes into the generation of kinetic energy. Since radiative-convective models do not consider generation of kinetic energy, Q_F is neglected. Since altitude is the only dimension considered in the model, the horizontal heat transport given by the second term on the left-hand side of (6) is neglected. This assumption is made with one or both of the following justifications: (1) this term is negligible, or (2) the primary interest is in the horizontally, i.e., latitudinally and longitudinally, averaged temperature and energy balance. *Gierasch and Goody* [1968] argue that justification 1 is applicable to Mars, and hence they apply the radiative-convective model to individual latitude zones of Mars. For the earth's atmosphere, however, this term and the $\rho g W$ term represent the dominant heat transport mechanism within the troposphere. Hence for the earth's atmosphere the model is used only in a horizontally averaged sense. Upon averaging (6) with respect to latitude and longitude and denoting the averaged quantities with angle brackets we have

$$\frac{\partial \langle \rho c_p T \rangle}{\partial t} = -\frac{d}{dz}(q_T + q_S + q_c) \tag{7}$$

where $q_c = \langle \rho c_p W T \rangle$ is the convective flux. The horizontal divergence terms in (6) drop out in the averaging process, and further, $\langle \rho g W \rangle = 0$ to satisfy mass conservation. Contributions to q_c can arise from both thermal convection and vertical motions resulting from global scale circulation in the atmosphere. The latter process is neglected in the model, and this assumption cannot be completely justified. The nonlinear effects of atmospheric circulation and the exchange of heat between oceans and atmosphere exert a strong influence on the seasonal march of atmospheric and surface temperatures, and since (7) does not incorporate such effects, the model applies for annually averaged 'steady state' conditions. By assuming that such a steady state exists, (7) can be integrated to yield

$$q_T(z) + q_S(z) + q_c(z) = \text{const} = 0 \tag{8}$$

with the boundary conditions

$$q_T(\infty) + q_S(\infty) = 0 \qquad q_c(\infty) = 0$$

Since W should vanish at the top of the atmosphere, $q_c(\infty) = 0$. The quantity $q_T(\infty)$ is the thermal radiation emitted to space by the earth-atmosphere system, and $q_S(\infty)$ is the difference between the incoming solar radiation and the solar radiation which is reflected to space by the system; i.e., $q_S(\infty)$ is the total solar radiation absorbed by the planet as a whole. Equation (8) is a statement of the fact that on a long-term average the net solar radiation absorbed by the planet is in balance with the radiation emitted to space by the planet. If this balance does not exist, the planet as a whole would be continuously warming or cooling, as the case may be. Equation (8) also states that on a time-, longitude-, and latitude-averaged basis, radiation and convection are the only two processes that determine the vertical thermal structure of the planet.

3. *Convective Adjustment*

Equations (7) and (8) do not fully define the problem; they only define the thermodynamic constraint on the system. The formulation of q_T and q_S in terms of temperature and the optically active atmospheric gases is straightforward, although it is quite complex. A discussion of the various methods of formulating and solving for the radiative fluxes is given in the next section. Here we will be mainly concerned with the formulation for the convective flux. An exact treatment for q_c would require the solution of the equations of motion and continuity in addition to the solution of the energy equation. This ambitious task has not been attempted by any of the radiative-convective models. In general, q_c is accounted for by semiempirical or empirical techniques.

The semiempirical techniques employ the mixing length hypothesis to treat the heat flux due to the convective elements. The mixing length theory assumes that the dominant mode of heat transport is by the turbulent eddies that have length scales which are much smaller than the characteristic length scales of the problem. With this assumption, q_c can be formulated in terms of a Fickian type diffusion equation

$$\begin{aligned} q_c &= -\rho c_p K_H \left(\frac{dT}{dz} + \Gamma\right) \qquad \frac{dT}{dz} + \Gamma \le 0 \\ q_c &= 0 \qquad\qquad\qquad\qquad \frac{dT}{dz} + \Gamma > 0 \end{aligned} \tag{9}$$

where K_H is the thermal diffusivity. The heat flux is assumed to be proportional to the gradient of the potential temperature: $(d\theta/dz) \propto [(dT/dz) + \Gamma]$. This theory of free convection was originated by *Priestley* [1959]. By invoking similarity arguments, Priestley showed that K_H was given by

$$K_H = 1.32 z^2 \left(\frac{|(dT/dz) + \Gamma| g}{T}\right)^{1/2} \tag{10}$$

Gierasch and Goody [1968] adopted (9) and (10) for a radiative-convective model study of the atmosphere of Mars. Their model study showed that within the convective region, i.e., the region where the radiative equilibrium lapse rate was superadiabatic, the temperature gradient was almost adiabatic, i.e., $(dT/dz) + \Gamma \approx 0$. More recent work on the formulation of K_H can be found in the papers of *Deardorff and Willis* [1967] and *Dyer* [1965]. The discussions and laboratory experiments by Deardorff and Willis indicate that (10) may be inadequate for treating convective heat transport under realistic atmospheric conditions.

The empirical technique, unlike the semiempirical technique, does not treat the convective processes explicitly. Instead, the effects of convection are included implicitly by assuming that convection maintains a critical temperature lapse rate within the convective region. This critical lapse rate is the lapse rate at which the atmosphere is in a neutral state, i.e., is neither stable nor unstable with respect to convective processes. For an atmosphere in which condensation processes are unimportant the critical lapse rate is the adiabatic lapse rate.

The empirical technique considerably simplifies the procedure for solving the thermal structure of the atmosphere. Since the temperature gradient is prescribed within the troposphere, (8) need not be solved. Instead, the equation for the radiative equilibrium condition, i.e., $q_T + q_S = 0$, is solved with the proviso that the lapse rate at any level within the atmosphere should be less than or equal to the critical lapse rate. Whenever the radiative equilibrium lapse rate is greater than the critical lapse rate, the lapse rate is set equal to the critical lapse rate. This lapse rate adjustment has come to be known as convective adjustment.

4. *Models for Planetary and Stellar Atmospheres*

Thus far the discussions on the modeling methodology apply to the earth's atmosphere as well as to planetary and stellar atmospheres. From now on we will restrict our attention to the earth's atmosphere.

Before leaving the subject of planetary and stellar atmospheres it should be pointed out that radiative-convective models have been applied extensively in planetary and stellar atmosphere studies, and hence a very rich body of literature exists for these applications. We mention some of these references below.

For a general introduction to the subject of radiative and radiative-convective equilibrium the reader is referred to the books by *Goody* [1964*a*], *Ambartsumyan* [1958], and *Chandrasekhar* [1957]. A very detailed review of the state-of-the-art thermal convection theories can be found in the review by *Spiegel* [1971].

Radiative-convective models for the atmospheres of Mars and Venus have been developed by *Gierasch and Goody* [1968], *Cess* [1972], and several others. *Cess and Khetan* [1973], *Cess and Chen* [1975], *Trafton* [1967], and *Wallace et al.* [1974] have developed models for the atmospheres of major planets. The analyses of Cess and his co-workers employ the empirical technique of convective adjustment and, perhaps for the first time, present a completely analytical solution for the radiative-convective equilibrium temperature profile of a nongray atmosphere. Their analyses clearly show that in a nongray atmosphere, when the centers of the individual spectral lines are saturated (i.e., optically thick), the temperature gradient should be continuous at the tropopause. A more general class of radiative-convective models which account for convective overshoot has been developed by *Gierasch* [1971] for the atmosphere of Mars.

We would like to caution the reader that the references to the planetary and stellar atmosphere applications mentioned here are by no means exhaustive. However, most of the references given here present summaries of the previous studies, and hence it is possible for the interested reader to compile a bibliography from these references.

C. Evaluation of Solar and Long-Wave Radiative Fluxes

As was described earlier, the distribution of long-wave and solar radiative fluxes within the model determines the radiative-convective equilibrium temperature profile. The lapse rate of this equilibrium profile is constrained to be less than or equal to a preassigned critical lapse rate. When the lapse rate is subcritical, radiative equilibrium applies; i.e., $q_s + q_T = 0$. When a layer in radiative equilibrium acquires a supercritical lapse rate, the layer undergoes convective adjustment; the lapse rate is set equal to the critical lapse rate. Radiative equilibrium need not apply within layers that have critical lapse rates, but it must apply at the boundaries of these layers if it is to apply at the top of the model atmosphere. An exception, of course, is that radiative equilibrium need not apply at the earth's surface if the lowest atmospheric layer undergoes convective adjustment.

In turn the radiative fluxes are composed of contributions from radiative sources at the boundaries of the model atmosphere and also from thermal emission by gases, clouds, and aerosols. The radiation from these sources is modified by absorption and scattering within the atmosphere. Thus the radiative fluxes that determine the equilibrium temperature profile depend on the radiative sources, the atmospheric composition, and, most important, the temperature profile itself. The fluxes are related to these factors through the equation of radiative transfer.

1. Absorption and Emission of Long-Wave Radiation

At small wave numbers $\nu = 1/\lambda \leq 2500\ \text{cm}^{-1}$ ($\lambda \geq 4\ \mu\text{m}$) the extinction of radiation due to scattering in the earth's atmosphere is small in comparison with the extinction due to absorption, and as a result the scattering of long-wave radiation is often neglected altogether. In addition, at these wave numbers the intensities of solar radiation are small in comparison with those of the radiation emitted by the atmosphere and the earth's surface; consequently, the earth's thermal emission can be taken as the sole source of long-wave radiation. At altitude z in a vertical column model the net flux of long-wave radiation for wave number interval $\Delta\nu_i$ is given by

$$q_i(z) = \pi B_i(0) T_i(z, 0) + \int_0^\infty \pi B_i(z')\, dT_i(z', z) \qquad (11)$$

Here $\pi B_i(z)$ is the spectrally averaged value of the Planck function:

$$\pi B_i(z) = \frac{1}{\Delta\nu_i} \int_{\Delta\nu_i} d\nu \pi B_\nu(z) \qquad (12)$$

where $\pi B_\nu(z)$ is the Planck function for wave number ν and temperature $T(z)$; $T_i(z, z')$ is the spectrally averaged flux transmissivity:

$$T_i(z, z') = \frac{1}{\Delta\nu_i} \int_{\Delta\nu_i} d\nu T_\nu(z, z') \qquad (13)$$

where $T_\nu(z, z')$ is the monochromatic flux transmissivity between levels z and z' of the model atmosphere. The flux transmissivity is related to the transmissivity $\tau(z, z', \mu)$ by

$$T(z, z') = 2 \int_0^1 d\mu \mu \tau(z, z', \mu) \qquad (14)$$

where μ is the cosine of the angle between the ray path and the vertical. The total net long-wave radiative flux is obtained by summing the contributions from each spectral interval. The total net long-wave flux is given by

$$q_T(z) = \Sigma_i q_i(z) \Delta\nu_i \qquad (15)$$

Because the Planck function changes slowly with wave number for the temperatures of the earth's atmosphere, (11) is valid for rather large spectral intervals. Spectral intervals of 100 cm^{-1} are commonly used. Such intervals are sufficiently wide to encompass entire vibration-rotation bands, such as the 9.6-μm band of O_3.

Numerous models have been developed for spectrally averaged, or mean, transmissivities of gases for homogeneous paths (i.e., paths for which the molecular composition, temperature, and pressure are constant). Three examples of such models are described in Table 1. For the purpose of radiative-convective modeling a distinction must be made between two classes of models. The first class of models are based on the physical processes that influence line absorption and the distribution of absorption lines within bands. Included in this class are nonoverlapping line models [*Dickinson*, 1972], random models [*Goody*, 1964*a*; *Rodgers*, 1968, 1976], and correlation models [*Edwards and Menard*, 1964]. In principle, such models may be applied to conditions which involve changing line shapes, as occur in the stratosphere, and inhomogeneous paths. The second class of models are based almost entirely on laboratory measurements of absorption, and these models are called empirical models [*Manabe and Strickler*, 1964; *Manabe*

TABLE 1. Examples of Models for Mean Transmissivities and Equivalent Widths

Model	Parameter	Definition	Reference
$T = \exp\left[-\frac{SM}{\delta}\left(1+\frac{SM}{\pi\alpha_0 P/P_0}\right)^{-1/2}\right]$	S	mean line strength	*Rodgers and Walshaw* [1966]
	α_0	mean half width of pressure-broadened line at P_0	
	δ	mean line spacing	
$T = \exp\left\{\frac{-\pi\alpha_0 P/P_0}{2\delta}\left[\left(1+\frac{4SM}{\pi\alpha_0 P/P_0}\right)^{1/2}-1\right]\right\}$	S	same as above	*Rodgers* [1968]
	α_0	same as above	
	δ	same as above	
$W = 2A_0 \ln\left\{1+\frac{S_0 M/A_0}{2+\{SM/A_0[1+\delta/(4\alpha_0 P/P_0)]\}^{1/2}}\right\}$	S_0	band strength	*Cess and Ramanathan* [1972]
	A_0	bandwidth parameter	
	α_0	same as above	
	δ	same as above	

The equivalent width W is related to the mean transmissivity by $T = (1 - W/\Delta\nu)$. M is the column amount (e.g., molecules per square centimeter) of the absorbing gas, and P is the total pressure of the gas. These models are for bands of pressure-broadened lines. The line shape is assumed to be Lorentzian.

and Wetherald, 1967]. Although empirical models often reproduce laboratory observations better than do physically derived models, there is no theoretical framework for extending empirical models to atmospheric conditions which differ substantially from those of the laboratory. Perhaps the only justification for using empirical models in atmospheric applications is to show, as did *Stone and Manabe* [1968], that the results obtained with the empirical models agree with those obtained with physically derived models.

In radiative-convective models, long-wave radiative flux calculations are often simplified by using a diffusivity factor. With a diffusivity factor the flux transmissivity is approximated by $T_\nu(z, z') \sim \tau_\nu(z, z'; \langle\mu\rangle)$. Here $1/\langle\mu\rangle$ is the diffusivity factor, and it is usually set equal to 1.66. This approximation causes systematic errors in fluxes and cooling rates of no more than a few percent [*Rodgers and Walshaw,* 1966]. Though such errors may influence the equilibrium temperature profile of a radiative-convective model, because they tend to be systematic and small, they are not likely to affect the response of the profile to changes in atmospheric composition or external conditions.

2. *Absorption and Scattering of Solar Radiation*

For wave numbers larger than 2500 cm^{-1} the intensities of radiation emitted by the earth's atmosphere and surface are sufficiently small in comparison with the intensities of solar radiation that the earth's thermal emission may be neglected. Also, at these wave numbers, both scattering and absorption by molecules, aerosols, and clouds contribute significantly to the extinction of solar radiation. Consequently, the equation for the specific intensity of solar radiation at level z is given by

$$\mu\, dI_\nu(z, \mu)/dz = -\rho(z)[\sigma_\nu(z) + \kappa_\nu(z)]I_\nu(z, \mu) + \rho(z)\sigma_\nu(z)\frac{1}{2}\int_{-1}^{1} d\mu' P_\nu(z, \mu, \mu')I_\nu(z, \mu') \qquad (16)$$

Here $I_\nu(\mu)$ is the azimuthally symmetric component of the specific intensity of solar radiation at wave number ν propagating along the ray specified by $\mu = \cos\theta$, where θ is the angle between the ray direction and the vertical direction. Since only radiative fluxes are required in radiative-convective models, we need to consider only the azimuthally symmetric component of the specific intensity [*Chandrasekhar,* 1960]. The net solar radiative flux is related to the specific intensity by

$$q_\nu(z) = 2\pi\int_{-1}^{1} d\mu\mu I_\nu(z, \mu) \qquad (17)$$

In (16), κ_ν and $\sigma_\nu P_\nu(\mu, \mu')$ are defined by

$$\kappa_\nu = \frac{1}{\rho}\Sigma_i \rho_i \kappa_{\nu i}$$

$$\sigma_\nu P_\nu(\mu, \mu') = \frac{1}{\rho}\Sigma_i \rho_i \sigma_{\nu i} P_{\nu i}(\mu, \mu')$$

and

$$\frac{1}{2}\int_{-1}^{1} d\mu' P_\nu(\mu, \mu') = 1$$

Here ρ is the atmospheric density and for the ith radiatively active constituent, ρ_i is the density; $\kappa_{\nu i}$ is the absorption cross section per unit mass, and $\sigma_{\nu i}P_{\nu i}(\mu, \mu')$ is the scattering cross section per unit mass. In common terminology, κ_ν is the mass absorption coefficient, σ_ν is the mass scattering coefficient, and $P_\nu(\mu, \mu')$ is the scattering phase function.

Numerous analytic approximations and numerical procedures have been developed to solve (16) and (17) for the monochromatic net solar radiative flux $q_\nu(z)$. The numerical procedures have been reviewed recently by *Hansen and Travis* [1974]. These numerical procedures are rather complex, and when the net radiative flux integrated over all wave numbers is to be calculated, as it is in radiative-convective models, even the simple analytic approximations for $q_\nu(z)$ become numerical nightmares. For these reasons the solutions to (16) and (17) are seldom sought in radiative-convective model calculations. Instead, several parameterizations have evolved for the net solar radiative flux in the earth's atmosphere [*Manabe and Strickler,* 1964; *Sasamori et al.,* 1972; *Lacis and Hansen,* 1974].

In these parameterizations the effects of scattering are often allowed for by assigning reflectivities and transmissivities to scattering layers. A scattering layer might consist of a cloud or an aerosol. The details of the radiation field within a scattering layer are then ignored.

An example of a parameterization is illustrated with the aid of Figure 1. The net flux of solar radiation at level z_1 is

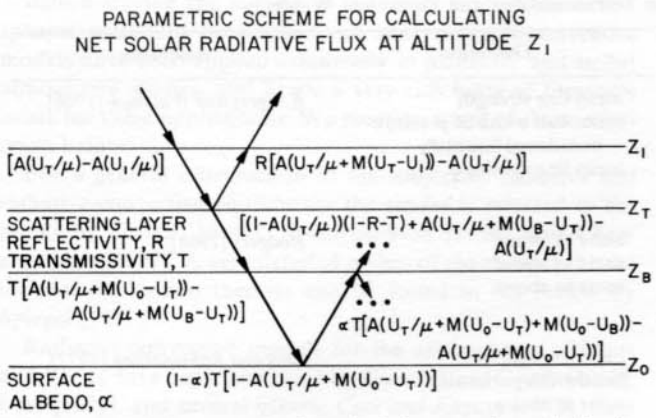

Fig. 1. Parametric scheme for calculating net solar radiative flux at altitude z_1: $A(W)$ is the absorption for optical path W, U_i is the absorber amount between level z_i and space, μ is the cosine of the solar zenith angle, and M is a diffusivity factor for scattered radiation.

equivalent to the flux of solar radiation absorbed below z_1. With reference to the figure the atmospheric absorption below z_1 is given by the following series:

$$\begin{aligned} A_{z_1} = {} & [A(U_T/\mu) - A(U_1/\mu)] + R[A(U_T/\mu \\ & + M(U_T - U_1)) - A(U_T/\mu)] \\ & + [(1 - A(U_T/\mu))(1 - R - T) \\ & + A(U_T/\mu + M(U_B - U_T)) - A(U_T/\mu)] \\ & + T[A(U_T/\mu + M(U_0 - U_T)) \\ & - A(U_T/\mu + M(U_B - U_T))] \\ & + \alpha T[A(U_T/\mu + M(U_0 - U_T) \\ & + M(U_0 - U_B)) - A(U_T/\mu + M(U_0 - U_T))] \end{aligned} \quad (18)$$

In (18), $A(W)$ is the absorption of solar radiation by an atmospheric gas in terms of the optical path W traversed by the radiation. For example, U_i is the optical path of the absorber for a vertical path from level z_i to space. The cosine of the zenith angle for the incident solar radiation is μ, and an effective cosine $1/M$ or diffusivity factor M is used to evaluate effective optical paths for scattered radiation. Radiation is assumed to be diffuse as soon as it contacts a scattering layer. The scattering layer in Figure 1 has been assigned a reflectivity R and transmissivity T. Its absorptivity is $1 - R - T$. The reflectivity of the surface, or surface albedo, is α.

In principle, the series (18) may be continued indefinitely, thereby incorporating the contributions to atmospheric absorption due to radiation reflected several times between the scattering layer and the surface. In practice, however, the series is terminated with the absorption of radiation that has been reflected only once, as was done above. Additional paths contribute little to atmospheric absorption, particularly when the surface albedo is small ($\alpha \sim 0.1$–0.2), as it is in radiative-convective models.

To obtain the total absorption below z_1, the absorption by the surface must be added to that by the atmosphere. The absorption by the surface is given by another series, the first term being

$$A_s = (1 - \alpha)T[1 - A(U_T/\mu + M(U_0 - U_T))] \quad (19)$$

Again, additional terms of this series give the contributions due to multiple reflections between the scattering layer and the surface. These terms may also be neglected provided the surface albedo is small.

As was mentioned earlier, because of their complexity, procedures for directly solving (16) and (17) are often avoided in radiative-convective model calculations. Nevertheless, when these procedures are used, further difficulties arise because (16) and many of the procedures used to solve it are valid only for monochromatic radiation. If (16) and procedures for solving it are to be applicable for finite spectral intervals, then the absorption must be represented by

$$A(u) = 1 - \Sigma_n P_n e^{-\kappa_n U} \quad (20)$$

Such a model is called an exponential sum-fit model. The p_n are said to represent the probability distribution of absorption coefficients κ_n within the finite spectral interval under consideration. The p_n and κ_n in (20) are often obtained by fitting the expression to either laboratory measurements of absorption or other band models [*Wiscombe and Evans*, 1977]. One further difficulty, however, remains for atmospheric paths. Although (20) may be justified for homogeneous scattering and absorbing media, its effectiveness has yet to be studied for inhomogeneous paths.

One procedure for solving the equation of radiative transfer which avoids these difficulties is the method of successive orders of scattering [*Hansen and Travis*, 1974]. Provided $\sigma_\nu P_\nu(\mu, \mu')$ changes slowly with ν, as is often the case, it is simple to show that the successive orders of scattering procedure is not constrained to monochromatic radiation; therefore band models of the form of (20) are not required. Instead, any band model, whether theoretical or empirical, may be used with this method. In addition, procedures for extending band models to accommodate inhomogeneous paths may also be used. Furthermore, since the method readily allows for emission in the presence of scattering, it may be used to treat scattering of long-wave radiation by clouds and aerosols. So far, only *Wang and Domoto* [1974] have employed a procedure similar to the successive orders of scattering method to solve the equation of transfer in a radiative-convective model.

3. *Transmission for Inhomogeneous Optical Paths*

As was mentioned earlier, most models of molecular transmissivity are derived either from theoretical considerations assuming homogeneous media or from laboratory measurements of transmission through homogeneous media. Optical paths in the atmosphere are, however, inhomogeneous. Gas pressures and mixing ratios of the optically active constituents may change by several orders of magnitude along an atmospheric optical path, while temperatures change by 30%. Since molecular transmissivity can be a rather sensitive function of pressure, partial pressure, and temperature, either the transmission models must be altered so that they allow for inhomogeneities or the inhomogeneous path must be replaced by some approximately equivalent homogeneous path or some equivalent combination of homogeneous paths. In radiative-convective models, inhomogeneous optical paths are usually replaced by equivalent homogeneous paths.

The Curtis-Godson approximation (and variants of it) is the most widely used procedure for replacing an inhomogeneous optical path with an equivalent homogeneous optical path [*Goody*, 1964*a*]. In the troposphere the width of spectral lines is proportional to the molecular collision frequency. As a result the transmission for an optical path depends on both the total amount of absorber in the path and the pressure along

the path. In the Curtis-Godson approximation the total absorber amount U and the equivalent pressure P for the path are defined by

$$U = \int \rho(z)\, dz \tag{21}$$

and

$$P = \frac{\int p(z)\rho(z)\, dz}{\int \rho(z)\, dz} \tag{22}$$

Here $\rho(z)$ is the density of the absorbing constituent and $p(z)$ is the atmospheric pressure along the path. These definitions are designed so that the absorption of a weak line (which is proportional to U) and that of a strong pressure-broadened line (which is proportional to $(UP)^{1/2}$) for the inhomogeneous path are exactly equal to the absorption of the weak and strong lines for a homogeneous path with amount U and pressure P. The accuracy of this approximation has been investigated [*Walshaw and Rodgers,* 1963; *Goody,* 1964*b*; *Armstrong,* 1968; *Kuriyan et al.,* 1977], and the approximation has been found to be accurate for most atmospheric applications. A notable exception, however, is the evaluation of cooling rates for the 9.6-μm band of ozone [*Walshaw and Rodgers,* 1963]. This matter is discussed later in section F*4*.

Scaling laws which resemble the Curtis-Godson approximation are often employed to evaluate equivalent homogeneous paths for empirical band models. If, for example, the transmission can be fitted to a function of a single variable,

$$W = U(P/P_0)^{\kappa} \tag{23}$$

then in a manner analogous to the Curtis-Godson approximation the variable for an inhomogeneous path is given by

$$W = \int (P(z)/P_0)^{\kappa}\, dU(z) \tag{24}$$

This method was used by *Manabe and Strickler* [1964] and by *Manabe and Wetherald* [1967] in their radiative-convective models. The procedure cannot, however, be justified from physical principles; nevertheless, *Stone and Manabe* [1968] have shown that results obtained by using such scaling laws agree with those obtained by using the Curtis-Godson approximation and physically derived band models.

4. *Miscellaneous Details*

a. Line shape. So far, radiative-convective models are usually constructed with the assumption that the molecular spectral lines are collision broadened and have Lorentz shapes. Molecular collisions are the predominant cause for line broadening in the lower part of the earth's atmosphere, where the pressure, and therefore the molecular collision frequency, is high. Above 40 km, however, the pressure in the earth's atmosphere is sufficiently low that the lines within some of the bands that contribute significantly to the long-wave cooling of the atmosphere no longer have Lorentz shapes. As the pressure decreases, their shapes change from Lorentz to Voigt (a convolution of Lorentz and Doppler shapes) and then to Doppler. Models extending to these levels need to allow for these more general line shapes. S. Manabe and R. T. Wetherald (private communication, 1978) account for the change in line shape for CO_2 in a more recent version of their earlier model [*Manabe and Wetherald,* 1967], and *Ramanathan* [1976] includes these effects for CO_2 and O_3. In section F*4* the error in cooling rate profiles obtained by using a Lorentz line shape instead of the correct Voigt or Doppler shape is investigated.

b. Emissivities. Because 20 or so spectral intervals are required to model the radiative properties of the rotation and the 6.3-μm bands of water vapor, long-wave radiative flux calculations are long and tedious. A popular method for reducing the computational task is to use an emissivity formulation for the long-wave absorption by water vapor [*Manabe and Strickler,* 1964; *Ramanathan,* 1976].

Separating (11) into the components for upward and downward fluxes gives

$$q_i^{+}(z) = \pi B_i(0) T_i(z, 0) + \int_0^z \pi B_i(z')\, dT_i(z', z) \tag{25}$$

for the upward flux and

$$q_i^{-}(z) = \pi B_i(z_0)[T_i(z, z_0) - T_i(z, \infty)] + \int_{z_0}^z \pi B_i(z')\, dT_i(z', z) \tag{26}$$

for the downward flux. Here $q_i(z) = q_i^{+}(z) - q_i^{-}(z)$ and z_0 is the lower boundary of an isothermal layer assumed to exist at the top of the model atmosphere. By using absorptivities $A_i(z, z') = 1 - T_i(z, z')$, (25) and (26) may be rewritten as follows:

$$q_i^{+}(z) = \pi B_i(0) + \int_0^z A_i(z, z')\, d\pi B_i(z') \tag{27}$$

and

$$q_i^{-}(z) = \pi B_i(z_0)\, A_i(z, \infty) + \int_{z_0}^z A_i(z, z')\, d\pi B_i(z') \tag{28}$$

With these expressions the total upward and downward long-wave radiative fluxes become

$$q^{+}(z) = \pi B(0) + \int_0^z \tilde{\epsilon}(z, z')\, d\pi B(z') \tag{29}$$

and

$$q^{-}(z) = \pi B(z_0)\, \epsilon(z, \infty) + \int_{z_0}^z \tilde{\epsilon}(z, z')\, d\pi B(z') \tag{30}$$

where the emissivities are given by

$$\tilde{\epsilon}(z, z') = \Sigma_i A_i(z, z') \frac{dB_i(z')}{dB(z')} \tag{31}$$

and

$$\epsilon(z, z') = \Sigma_i A_i(z, z') \frac{B_i(z')}{B(z')} \tag{32}$$

and were $\pi B(z)$ is the integral of the Planck function over all wave numbers: $\pi B(z) = \sigma T^4(z)$.

In order to realize a significant reduction in computing time when using emissivities, simple parameterizations must be developed for ϵ and $\tilde{\epsilon}$. Usually, ϵ and $\tilde{\epsilon}$ are parameterized to be functions of water vapor amount, mean pressure, and mean temperature for the optical path. Such parameterizations lose the spectral variation of the temperature and pressure dependencies of the optical constants. Often the temperature dependence is entirely neglected. The neglect of the temperature dependencies is the major contribution to the errors encountered when using emissivities. Dropping the temperature dependence of the optical constants for the rotation band of water vapor [*Rodgers and Walshaw,* 1966] gives errors of as much as 20% in the cooling rates of the lower tropospheric layers and 5% in the downward long-wave flux at the surface. A further approximation is to assume that the water vapor

absorption lines are in a strong line limit. In this limit, ϵ and $\tilde{\epsilon}$ are functions of the product of the water vapor amount and the Curtis-Godson pressure, (22). The error contributed by this approximation is negligible in comparison with that contributed by neglecting the temperature dependence of the optical constants. Such errors are generally systematic, and thus they are not likely to affect a radiative-convective model's sensitivity to changes in atmospheric composition or external conditions. Nevertheless, such errors may be reduced by using a combination of band models and emissivities, as described by *Fels and Schwarzkopf* [1975].

With the formulation given here, two emissivities, ϵ and $\tilde{\epsilon}$, are required to evaluate the net long-wave radiative flux, and only one of these, ϵ, can be measured in the laboratory [*Rodgers*, 1967]. The other must be evaluated from theoretical models (e.g., band models) of the absorption due to water vapor.

Instead of (29) and (30), *Ramanathan* [1976] used

$$q^+(z) = \pi B(0)[1 - \epsilon(z, 0)] - \int_0^z \pi B(z')\, d\hat{\epsilon}(z, z') \tag{33}$$

and

$$q^-(z) = \pi B(z_0)[\epsilon(z, \infty) - \epsilon(z, z_0)] - \int_{z_0}^z \pi B(z)\, d\hat{\epsilon}(z, z') \tag{34}$$

Here $\hat{\epsilon}(z, z')$ is given by [*Rodgers*, 1967]

$$\hat{\epsilon}(z, z') = \int_z^{z'} dz'' \frac{\pi B_\nu(z'')}{\pi B(z'')} \frac{dA_\nu(z'', z)}{dz''} \tag{35}$$

Like $\tilde{\epsilon}(z, z')$, $\hat{\epsilon}(z, z')$ must also be derived theoretically.

D. Solving for the Equilibrium Temperature Profile

Two methods have been developed for obtaining the temperature profile which satisfies the conditions of radiative-convective equilibrium. The first is a time-stepping method [*Manabe and Strickler*, 1964; *Manabe and Wetherald*, 1967]. This method is intuitively obvious but numerically inefficient. The second is a Newton-Raphson method, and it is considerably more efficient than the time-stepping method [*Ramanathan*, 1976; *Coakley*, 1977*a*].

1. *Time-Stepping Method*

The time-stepping method begins with an initial guess of the equilibrium temperature profile. The initial guess need not be realistic. So far the equilibrium temperature profiles of radiative-convective models have proven to be insensitive to the choice of the initial temperature profile [*Manabe and Strickler*, 1964]. The model atmosphere is divided into layers, and the net radiative heating rates are evaluated for each layer. The net radiative heating rate of the layer centered about z_k is given by

$$\frac{dT_0(z_k)}{dt_0} = \frac{g}{c_p}\left[\frac{\Delta q_S(z_k)}{\Delta P} + \frac{\Delta q_T(z_k)}{\Delta P}\right] \tag{36}$$

where g is the acceleration due to gravity, c_p is the specific heat at constant pressure, $\Delta q(z_k)$ is the net radiative flux at the top of the layer minus the net radiative flux at the bottom of the layer, and ΔP is the pressure at the top of the layer minus the pressure at the bottom of the layer. At the next time step $t_1 = t_0 + \Delta t$ the temperature profile is determined from the initial temperature profile and the net radiative heating rates for the layers. The temperature of the layer centered about z_k is given by

$$T_1(z_k) = T_0(z_k) + \frac{dT_0(z_k)}{dt_0}\Delta t \tag{37}$$

The new temperature profile is then used to compute new heating rates which in turn are used to obtain the temperature profile for the next time step. This procedure is repeated until the net radiative heating of each model layer not subject to convective adjustment and the net radiative fluxes at the top of convective layers are sufficiently small that the conditions of radiative-convective equilibrium are closely satisfied.

During the course of these iterations, convective adjustment is invoked whenever radiation forces the temperature difference between two adjacent layers to become greater than the difference that would exist with the preassigned critical lapse rate. In the adjustment procedure the temperature of the upper of the two layers is altered so that it is consistent with the critical lapse rate. During subsequent time steps the temperature difference between these two layers is fixed by the critical lapse rate, and the two layers together effectively become a single layer in radiative equilibrium.

The time-stepping procedure may require several hundred iterations of the radiative flux and heating rate calculations before equilibrium is achieved. *Manabe and Strickler* [1964] used an 8-hour time step in order to avoid numerical instabilities. With this time step, approximately 200 model days or 600 iterations were required for the model to reach equilibrium. *Manabe and Wetherald* [1967] found that approximately the same number of model days were also required for the model to reach equilibrium from temperature profiles that differed from the equilibrium profile by only +15°C and −15°C at each of the model levels. Because of the large number of iterations the time-stepping procedure has been unattractive for solving models that employ complex radiative transfer calculations or that include other physical processes such as chemical reactions and kinetics.

2. *Newton-Raphson Method*

To reach the equilibrium temperature profile, the Newton-Raphson method typically requires from three to five iterations of the radiative calculations. It is therefore considerably more efficient than the time-stepping procedure.

The method follows from the Curtis matrix formulation of long-wave cooling. In this formulation the long-wave cooling of layer z_k is given by

$$C(z_k) = \Sigma_{ij}\, D_{ikj} B_i(z_j) \tag{38}$$

where, as in section C1, $B_i(z_j)$ is the average value of the Planck function for the ith spectral interval, and it is evaluated at the temperature of level z_j. The matrix D_{ikj} in (38) is the Curtis matrix for the ith spectral interval [*Rodgers and Walshaw*, 1966]. By assuming that the temperature dependencies of the elements in the Curtis matrix are small in comparison with those of the $B_i(z_j)$ the long-wave cooling rates may be expressed by using the following Taylor series expansion:

$$C(z_k) = C_0(z_k) + \Sigma_j G_{kj}(T_j - T_{j_0}) \tag{39}$$

where

$$G_{kj} = \Sigma_i\, D_{ikj} \left.\frac{dB_i(z_j)}{dT_j}\right|_{T_{j_0}} \tag{40}$$

A radiative equilibrium temperature profile is obtained by solving

$$H(z_k) + C_0(z_k) = -\Sigma_j G_{kj} (T_j - T_{j_0}) \quad (41)$$

for T_j. Since the matrix elements G_{kj}, the long-wave cooling rates for the initial guess temperature profile $C_0(z_k)$, and the solar heating rates $H(z_k)$ all depend on the atmospheric temperature profile, (41) is solved sequentially to obtain the radiative equilibrium temperature profile.

The procedure just outlined is readily extended to include layers that undergo convective adjustment. These layers are identified by the supercritical gradients of their radiative equilibrium temperature profiles, and as is done with the time-stepping procedure, the layers are found by trial and error. Because radiative equilibrium is not maintained within them, the layers of the model which undergo convective adjustment must be removed from (41). At the same time the net solar and long-wave radiative fluxes must cancel at the top boundaries of the convective zones. An expression similar in form to (38) also applies to the net long-wave radiative flux. Thus only the G_{kj} require modification so that the temperatures of convective layers are constrained to the critical lapse rate.

To illustrate the procedure, suppose level m is the top of a convective region which consists of the model layers $n \leq \ell \leq m - 1$, i.e., level m is the upper boundary of level $m - 1$. These layers need not satisfy the condition of radiative equilibrium, and therefore (41) does not apply for $n \leq k \leq m - 1$. If the net solar radiative flux is to cancel the net long-wave radiative flux at the top of the model atmosphere, however, then the net solar radiative flux must also cancel the net long-wave radiative flux at level m. This cancellation is achieved by including with the equations for the layer heating an equation for the net radiative flux at level m. The net radiative flux is given by

$$q_S(z_m) + q_T(z_m) = -\Sigma_j G_{mj}(T_j - T_{j_0}) \quad (42)$$

where it is understood that G_{mj} is derived from the Curtis matrix used for net long-wave radiative fluxes rather than from the Curtis matrix used for long-wave radiative cooling rates. Because the equations for layers $n \leq \ell \leq m - 1$ have been removed from the equations for the radiative heating of the layer and because only one additional equation, (42), has been added, only one of the level temperatures within the convective zone can be obtained by inverting the resulting system of equations. Suppose this temperature is that of level m, T_m. Of course, the temperatures within the convective region affect both the long-wave radiative flux at level m and the cooling of the other atmospheric layers. To allow for this influence, the matrix elements $G_{k\ell}$ with $n \leq \ell \leq m$ must be modified so that changes in the temperatures of the convective layers are reflected in the radiative fluxes and cooling rates. Since the lapse rate within the convective region is specified, the layer temperatures are linked to T_m. If the model levels have fixed altitudes, then $T_m - T_{m_0} = T_\ell - T_{\ell_0}$ with $n \leq \ell \leq m$ and the $G_{k\ell}$ with $n \leq \ell \leq m$ may be lumped into the matrix elements for level m, $\mathcal{G}_{km}$, given by

$$\mathcal{G}_{km} = \sum_{\ell=n}^{m} G_{k\ell} \quad (43)$$

If, on the other hand, the model levels have fixed pressures, then

$$(T_m - T_{m_0}) (P_m/P_\ell)^\kappa = T_\ell - T_{\ell_0} \quad (44)$$

where $\kappa = R\Gamma/g$, R is the gas constant, Γ is the critical lapse rate, and g is the acceleration due to gravity. In this case, $\mathcal{G}_{km}$ would be given by

$$\mathcal{G}_{km} = \sum_{\ell=n}^{m} G_{k\ell} (P_m/P_\ell)^\kappa \quad (45)$$

With these alterations, (41) becomes a set of equations for the radiative-convective equilibrium temperature profile.

Implicit in the Newton-Raphson method is the assumption that neither solar heating rates nor elements of the Curtis matrix are greatly influenced by the atmospheric temperature profile. The temperature dependencies of these quantities come from the temperature dependencies of the optical paths. These dependencies appear to be sufficiently small that including them in the evaluation of the solar heating rates and the elements of the Curtis matrix does not affect the number of iterations required to reach equilibrium [*Coakley*, 1977*a*]. Finally, although a stability analysis of the Newton-Raphson method has yet to be performed, no numerical instabilities have been encountered. The sensitivity of the equilibrium temperature profile to the choice of an initial guess temperature profile has been studied, and as is true with the time-stepping procedure, the equilibrium temperature profile obtained with the Newton-Raphson method is insensitive to the choice of the initial profile.

E. Models for the Earth's Climate

The first radiative-convective model for the earth's atmosphere was developed by *Manabe and Strickler* [1964]. It was followed by several other models [*Manabe and Wetherald*, 1967; *Wang and Domoto*, 1974; *Ramanathan*, 1976; *Coakley*, 1977*a*]. A subset of the radiative-convective models are the models that prescribe the temperature distribution within the stratosphere rather than compute the radiative equilibrium temperature distribution. The models of *Rasool and Schneider* [1971], *Cess* [1974, 1976], *Weare and Snell* [1974], and *Pollack et al.* [1976] fall into this category.

As was mentioned earlier, the models compute the horizontally and annually averaged global surface and atmospheric temperatures, and they adopt the previously mentioned empirical technique of convective adjustment within the troposphere. The temperature profile is determined basically by the vertical distribution of the solar and long-wave radiative fluxes which in turn depend on the vertical distribution of the optically active atmospheric gases, aerosols, and clouds and the optical properties of the surface, clouds, atmospheric gases, and aerosols. The most important of the optically active gases are the major trace species H_2O, CO_2, and O_3. The atmospheric distribution of H_2O, clouds, and the surface ice and snow cover (which determines in part the reflectivity of the surface) are strongly coupled to the surface and atmospheric temperatures. This mutual coupling between temperatures and the radiative components gives rise to several feedback mechanisms. We will first describe the external variables in the model and discuss next the feedback mechanisms. Here external variables are the ones that are held prescribed in the model to be independent of the surface and atmospheric temperatures.

1. *External Variables*

a. Solar radiation. The fundamental external variable is the incoming solar radiation S_0 at the top of the atmosphere. The value of S_0 is being revised periodically as more accurate measurements become available. The older value of S_0 is

1395.3 W m^{-2}, while recent measurements seem to converge on 1367 W m^{-2} [*Duncan et al.*, 1977]. We will adopt the value of 1360 W m^{-2}.

b. Clouds. Clouds have a significant influence on both the long-wave and the solar radiative fluxes. Clouds absorb, emit, and, to a limited extent, scatter long-wave radiation, while they absorb, scatter, and transmit solar radiation. The radiative properties of clouds are assumed to be wavelength independent in all the models with the possible exception of the model of *Wang et al.* [1976]. For long-wave radiation, clouds are assumed to be either black or semiblack, and for solar radiation the cloud reflectivity is generally assumed to be between 0.45 and 0.5. *Manabe and Wetherald* [1967] consider three cloud levels; all the other models consider a single cloud level. The total fractional cloud cover is usually assumed to be between 0.45 and 0.55.

c. Optically active gases. Until recently, H_2O, CO_2, and O_3 were the only major gases included in the models. However, some recent work has shown that other minor gases such as N_2O, CH_4, HNO_3, and CCl_4 have to be included in the models in order to calculate the long-wave fluxes to within 0.1%.

For H_2O, as was suggested by *Manabe and Wetherald* [1967], the relative humidity is fixed in the model. These authors suggested that the atmosphere tends to conserve relative humidity rather than to conserve absolute humidity. In support of their suggestion the authors compared the observed profiles of zonal mean relative humidity (drawn as a function of latitude and altitude) for winter and summer and noted the similarity between the two profiles. Although the two seasonal profiles resembled each other qualitatively, there are minor quantitative differences. *Manabe and Wetherald* [1967] obtained the hemispherical mean relative humidity profile from the observed zonal mean profiles and proposed the following simple profile to be adopted in radiative-convective models:

$$RH = 0.77[(A - 0.02)/(1 - 0.02)] \tag{46}$$

where $A = p/p^*$ and p^* is the surface pressure. The relative humidity predicted by (46) becomes negative when A is less than 0.02. Noting that the stratosphere is very dry at an average mass mixing ratio of about 3 ppm, we modify (46) by setting

$$\begin{aligned} f_w &= \frac{0.622RHe_S(T)}{p - RHe_S(T)} && f_w \geq 3 \text{ ppm} \\ f_w &= 3 \text{ ppm} && f_w < 3 \text{ ppm} \end{aligned} \tag{47}$$

where f_w is the mass mixing ratio of H_2O, $e_S(T)$ is the saturation vapor pressure of H_2O, and RH is given by (46). More recently, however, *Cess* [1976] suggested that RH should be a function of T_s. Cess's suggestion is based on the fact that the observed hemispherically averaged value of RH is larger in summer than in winter. *Cess* [1976] incorporated the surface temperature dependence of RH by letting

$$RH = RH^*[(A - 0.02)/(1 - 0.02)]^{\Omega} \tag{48}$$

$$\Omega = 1.0 - 0.03(T_S - 288) \tag{49}$$

where RH^* is the surface relative humidity.

The atmospheric distributions of CO_2 and O_3 are prescribed in the model. CO_2 is assumed to be mixed uniformly within the atmosphere at a mixing ratio of 320 ppm (by volume). For O_3 the models assume the observed mid-latitude distribution given by *Krueger and Minzner* [1976].

d. Tropospheric lapse rate. The models assume the critical lapse rate to be 6.5°K/km. This value was originally suggested by *Manabe and Strickler* [1964], and all of the models have adopted this value. Manabe and Strickler's suggestion is based on the fact that in the U.S. Standard Atmosphere (1962) the lapse rate within the troposphere is 6.5°K/km. All of these studies have implicitly assumed that the standard atmosphere lapse rate is representative of the lapse rate of the globally averaged atmosphere. But the lapse rate of the globally averaged atmosphere is significantly less than the standard atmosphere lapse rate. We will discuss this point in more detail later.

e. Remaining parameters. The optical properties of the surface are assumed to be independent of wavelength. In the long-wave region the surface is assumed to be black, i.e., the emissivity is 1. Although the long-wave emissivity is significantly different from 1 for some desert surfaces [*Prabhakara and Dalu*, 1976], the globally averaged emissivity should be close to 1 [*Sellers*, 1965, Tables 1–3]. For solar radiation the value assumed for the surface reflectivity is between 0.1 and 0.11. In addition, a mean value of $\frac{1}{2}$ is assumed for the cosine of the solar zenith angle, and the fractional day of sunshine is also assumed to be $\frac{1}{2}$.

2. Feedback Mechanisms

Here we consider the feedbacks that arise because of the interactions between T_S and RH and between T_S and cloud altitude.

a. Relative humidity feedback. Since the relative humidity is fixed in the model, an increase (or decrease) in T_S is accompanied by an increase (or decrease) in the concentration of water vapor in the atmosphere. The corresponding increase (or decrease) of the H_2O long-wave opacity and solar absorption amplifies the increase (or decrease) in T_S. As will be shown later, the relative humidity feedback nearly doubles the model surface temperature changes due to perturbations.

Until recently, it had been customary to keep the cloud top altitude fixed when changing T_S [e.g., *Manabe and Wetherald*, 1967; *Rasool and Schneider*, 1971]. More recently, *Cess* [1974] suggested an alternate cloud model, the fixed cloud top temperature (FCT) model, in which the cloud top temperature is held fixed instead of the cloud top altitude. It will be shown that the sensitivity of T_S to perturbations as yielded by the FCT model is much larger than that of the fixed cloud altitude (FCA) model.

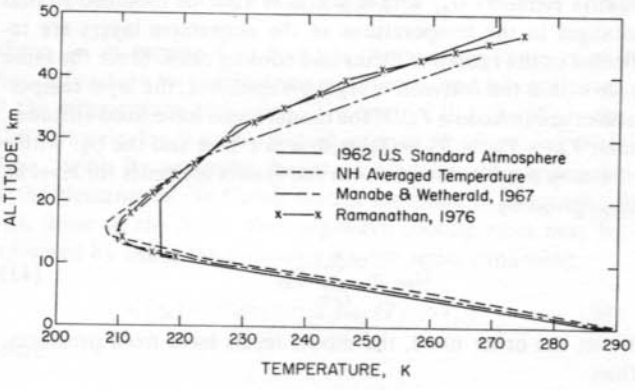

Fig. 2. Comparison of the radiative-convective model temperature profiles with observations. (NH is northern hemisphere.)

TABLE 2. Comparison of Hemispherical Mean Heat Balance Components

	Model Value	Observed Value: *London* [1956]	Observed Value: *Vonder Haar and Suomi* [1971]
Outgoing long-wave radiation at the top of the atmosphere	228	226	230
Net incoming solar radiation at the top of the atmosphere	228	226	237
Atmospheric long-wave heating	−168	−163	
Atmospheric solar heating	63	61	
Long-wave heating of the earth's surface	−60	−63	
Solar heating of the earth's surface	165	165	

The observed values are for the northern hemisphere. The model values are taken from *Manabe and Strickler* [1964]. The units of heat balance components are watts per square meter.

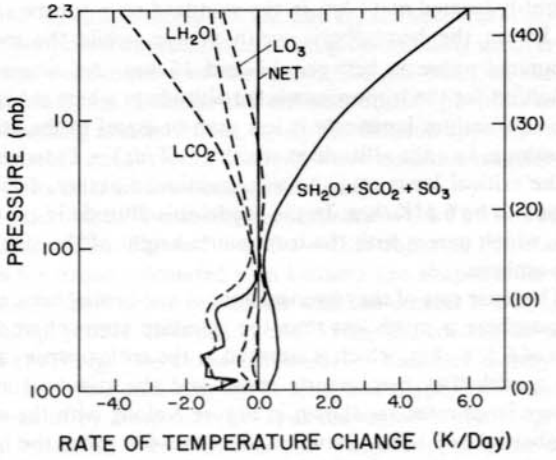

Fig. 4. Radiative-convective model results for the long-wave cooling and solar heating rates. The letters L and S denote long-wave and solar, respectively. The model results are taken from *Manabe and Strickler* [1964].

F. Model Studies of Present Climate

1. *Present Climate*

Since the model climate, defined by the surface and atmospheric temperatures, is primarily determined by radiative considerations, the model has been most useful in examining the mutual relationship between the vertical distribution of temperature and radiative fluxes. We will describe the various model results and examine the role of clouds, H_2O, CO_2, and O_3 in determining the global thermal structure and energy balance.

2. *Thermal Structure*

The temperature profile computed by the models of *Manabe and Wetherald* [1967] and *Ramanathan* [1976] are shown in Figure 2 along with the U.S. Standard Atmosphere (1962) and the annual hemispheric mean temperature profile of the northern hemisphere given by *Oort and Rasmusson* [1971]. The standard atmosphere temperature profile is strictly an annual mean profile for the mid-latitude and hence may not be representative of hemispheric mean conditions. In spite of this limitation it has become customary to compare the radiative-convective model profile (which represents hemispheric mean conditions) with the standard atmosphere. This procedure has led to some misinterpretations regarding the validity of radiative-convective model assumptions. The hemispheric mean profile of Oort and Rasmusson does not extend above 20 km. However, above 20 km the standard atmosphere profile is representative of hemispheric mean conditions.

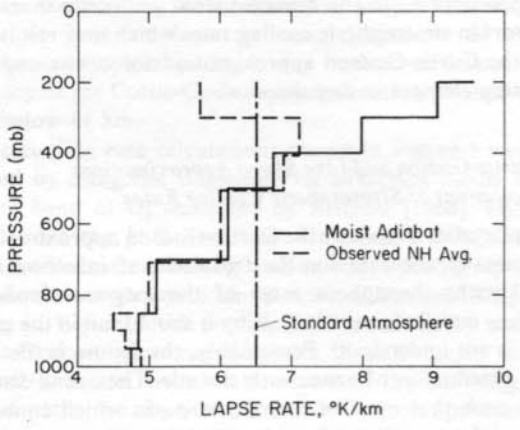

Fig. 3. Comparison of U.S. Standard Atmosphere (1962) lapse rate with observed northern hemisphere (NH) and moist adiabatic lapse rates. The NH values are taken from *Oort and Rasmusson* [1971].

Referring to Figure 2, we see that the computed stratospheric temperatures above 20 km are in remarkable agreement with the standard atmosphere. The close agreement can be considered as one indication that on a global mean basis the stratosphere above 20 km is in radiative equilibrium. A similar conclusion has been inferred from more detailed three-dimensional circulation model studies which include the combined effects of circulation and radiation [*Manabe and Hunt*, 1968]. The maximum discrepancy between the computed and standard atmospheres is in the lower stratosphere. The computed temperature at 13 km is colder by about 6°K. It is commonly believed that the effects of dynamics are important in this region and hence radiative equilibrium is a poor assumption for the lower stratosphere. The computed values, however, are in excellent agreement with the hemispheric mean profile. Although it is tempting to conclude from this agreement that the entire stratosphere is in radiative equilibrium on a hemispherically averaged basis, one cannot dismiss the possibility that the agreement may be fortuitous.

The surface temperature computed by Manabe and Wetherald is 288.4°K, in excellent agreement with the observed annual mean global value. The heat balance components computed by the model are shown in Table 2 along with the values obtained by *London* [1956] and by *Vonder Haar and Suomi* [1971] which represent annual mean conditions for the northern hemisphere. London obtains his values by computing the long-wave and solar radiative fluxes from observed values of temperature, clouds, and relative humidity. Vonder Haar and Suomi obtain their values from satellite measurements of the earth's radiation budget. It is seen from Table 2 and Figure 2 that the model reproduces the observed annual and hemispheric mean energy budget of the northern hemisphere.

The computed tropopause height is also in close agreement with the observed value. There are at least two commonly accepted definitions for the tropopause height. The first definition for the tropopause is the height at which the vertical temperature gradient changes abruptly in magnitude and possibly in sign. On the basis of this definition the tropopause

height is located at 11 km in the standard atmosphere and at 15 km in the hemispheric mean profile, while the model-computed value is between 14 and 16 km. An alternative definition for the tropopause is the altitude at which the radiative equilibrium lapse rate is less than or equal to the critical lapse rate, i.e., the altitude at which $(-dT/dz) = \Gamma_c$, where Γ_c is the critical lapse rate. As was mentioned earlier, Γ_c is assumed to be 6.5°K/km. In the model this altitude is about 11 km, which agrees with the tropopause height of the standard atmosphere.

The lapse rate of the observed annual and hemispheric mean troposphere is much less than the standard atmosphere lapse rate of 6.5°K/km, which is adopted as the critical lapse rate in the model. The hemispheric mean and the standard atmosphere lapse rates are shown in Figure 3 along with the moist adiabatic lapse rates. Between 1000 and 400 mbar the hemispheric mean lapse rate is almost equal to the moist adiabatic lapse rate, while between 400 and 200 mbar the hemispheric mean lapse rate is in much better agreement with the standard atmosphere. In summary, we need to revise the choices of the critical lapse rate parameter in radiative-convective models.

3. *Radiative Heating and Cooling*

The various radiative heating and cooling components computed by *Manabe and Strickler* [1964] are shown in Figure 4. The rates of temperature changes due to long-wave cooling by H_2O, CO_2, and O_3 are denoted by LH_2O, LCO_2, and LO_3, respectively, and the rates of temperature change due to solar heating by H_2O, CO_2, and O_3 are denoted by SH_2O, SCO_2, and SO_3, respectively. The net temperature change, as shown by the curve marked NET, is zero in the stratosphere (i.e., above 11 km), since this region is in radiative equilibrium. The troposphere is subject to a net radiative cooling. The convective adjustment implicitly assumes that this net cooling is compensated by the vertical transfer of heat from the surface by atmospheric motions (which includes planetary scale, baroclinic eddies, Hadley cells, and convection).

The relative importance of the radiative components varies with altitude. In the troposphere, H_2O contributes the most to long-wave cooling and solar heating, while in the stratosphere, CO_2 contributes the most to long-wave cooling, and O_3 contributes the most to solar heating. In the region between 10 and 20 km, all of these components are equally important. The 9.6-μm band of ozone causes a net heating in the region between 15 and 25 km. There is very little ozone in the troposphere, and hence most of the radiation emitted by the warmer surface penetrates through the troposphere. The bulk of the stratospheric ozone is in the region between 15 and 30 km. There it absorbs the 9.6-μm radiation emitted by the warmer surface and contributes to the radiative heating between 15 and 25 km.

On the basis of the radiative cooling and heating curves shown in Figure 4 it is possible to explain the globally averaged thermal structure of the atmosphere. Long-wave cooling by H_2O destabilizes the lower regions of the atmosphere, thereby causing supercritical lapse rates. Hence the water vapor opacity is the most important reason for the existence of the troposphere. The ozone solar heating, and to a limited extent the O_3 long-wave heating, causes the increase of temperature with altitude in the middle and upper stratosphere. The O_3 heating in the middle and upper stratosphere is essentially balanced by long-wave cooling due to the CO_2 15-μm bands. The minimum temperature at the tropopause is primarily due to a minimum in the solar heating at this level. Although Manabe and Strickler's calculations shown in Figure 4 illustrate the qualitative nature of the various radiative components, quantitatively, their results may not reflect the true globally averaged picture. The stratospheric mixing ratio of H_2O used in their calculations is too large. They neglect Doppler broadening effects which become important above 35 km. Furthermore, in the 15-μm region, CO_2 has several tens of hot and isotopic bands which contribute significantly to the cooling rates; it is not clear how these bands are treated in their model.

The evaluation of long-wave radiative cooling rates for the stratosphere is complex, and, as was implied above, approximations are often invoked to simplify these calculations. Perhaps the most commonly used are the Curtis-Godson approximation and the assumption of Lorentz line shapes. Both approximations can be invalid in the stratosphere. The Curtis-Godson approximation (cf. section C*3*) is suspected of being inadequate for the treatment of inhomogeneous optical paths in the 9.6-μm band of ozone [*Walshaw and Rodgers*, 1963; *Kuriyan et al.*, 1977]. Also, the shape of molecular absorption lines changes from Lorentz to Voigt and Doppler shapes in the upper stratosphere.

The changes in line shape have been included in several models that calculate only cooling rates from a prescribed temperature distribution [e.g., *Curtis*, 1956; *Murgatroyd and Goody*, 1958; *Kuhn and London*, 1969; *Drayson*, 1967; *Dickinson*, 1973]. Using the procedures developed by Curtis and by Murgatroyd and Goody, *Leovy* [1964] allowed for line shape changes in calculations of radiative-chemical equilibrium temperatures for the stratosphere and mesosphere. *Dickinson* [1972] has applied his model to calculate the equilibrium temperature of the Venusian mesosphere. These details, however, are often ignored in radiative-convective models. *Ramanathan* [1976] has explicitly allowed for the change in line shape for CO_2 and O_3 in a radiative-convective model, but his treatment is only approximate. In an improved version of the *Manabe and Wetherald* [1967] model these authors include the change in line shape for the CO_2 bands. They adopt the high-resolution theoretical transmission calculations of *Drayson* [1966]. Drayson performs a line-by-line integration, adopting intervals as narrow as 0.001 cm^{-1} over line centers and 0.1 cm^{-1} over line wings. The integration over inhomogeneous paths is performed exactly instead of by adopting the Curtis-Godson approximation. The Voigt line shape is used for pressures less than 0.1 atm. Drayson's transmission values can perhaps be considered as bench mark values for validating the approximate procedures. In the section below we briefly investigate the errors in stratospheric cooling rates which may result from using the Curtis-Godson approximation for ozone and from neglecting changes in line shape.

4. *Curtis-Godson and Line Shape Approximations in Calculations of Stratospheric Cooling Rates*

In spite of its simplicity the Curtis-Godson approximation is exceptionally accurate for the treatment of inhomogeneous optical paths throughout most of the long-wave spectrum [*Walshaw and Rodgers*, 1963]. Why it should fail in the case of ozone is not understood. Presumably, the failure is the result of the distribution of ozone with altitude. The ozone distribution is such that most of the optical paths which contribute significantly to radiative fluxes and cooling rates are in neither a strong nor a weak line limit. While the Curtis-Godson approximation is exact for optical paths that are in either strong

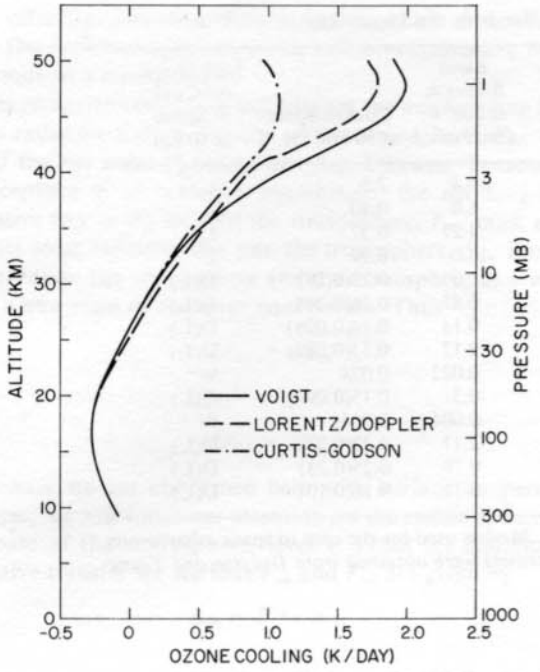

Fig. 5. Ozone cooling rates calculated using three methods: exact treatment of inhomogeneous optical path employing Voigt line shapes (solid curve); exact treatment of inhomogeneous optical path employing Lorentz and Doppler line shapes as suggested by *Ramanathan* [1976] (dashed curve); and Curtis-Godson treatment of inhomogeneous path employing Lorentz line shape (dashed-dotted curve). See text for further details of the calculations.

or weak line limits, it is only approximately correct for optical paths that are intermediate.

To illustrate the accuracy of the Curtis-Godson approximation, Figure 5 shows cooling rates calculated for the 9.6-μm band of ozone by using three methods: an exact calculation employing the Voigt profile for the line shapes (solid curve), an approximate calculation with the Curtis-Godson approximation employing the Lorentz profile for the line shapes (dashed-dotted curve), and a second approximate calculation employing both Lorentz and Doppler profiles for the line shapes as suggested by *Ramanathan* [1976] but with an exact treatment of the inhomogeneous paths (dashed curve). Ramanathan suggests that below approximately 41 km, Lorentz shapes should be used for ozone absorption lines, while above, Doppler shapes should be used. His reasons will be explained below. Because the cooling for Lorentz line shapes (dashed curve below 41 km) employs an exact treatment of the inhomogeneous optical paths, it may be used to determine the accuracy of the Curtis-Godson approximation (dashed-dotted line) below 41 km.

The cooling rate calculations shown in Figure 5 were performed by using the single-interval Malkmus model for the 9.6-μm band of O_3 described by *Rodgers* [1968]. For these calculations the U.S. Standard Atmosphere (1962) temperature profile was used along with an ozone profile representative of mid-latitude conditions [*Lacis and Hansen,* 1974]. Comparing in Figure 5 the cooling rates obtained by using the Curtis-Godson approximation with those obtained by using Lorentz lines and an exact treatment of the inhomogeneous optical paths, we see that the Curtis-Godson approximation contributes at most a 0.1°K/d error in the cooling rate. Although such errors may be a large percentage of the ozone cooling, they are small in comparison with the total cooling, 1.5°–2°K/d, due to H_2O, CO_2, and O_3 at these altitudes. The Curtis-Godson approximation also gives similarly small errors for the contribution of the ozone 9.6-μm band to the net radiative fluxes. Because the errors are small portions of the total cooling and net fluxes, the Curtis-Godson approximation is probably adequate for the long-wave radiative transfer calculations in radiative-convective models.

In addition to illustrating the accuracy of the Curtis-Godson approximation, Figure 5 also shows that above 40 km, cooling rates for ozone calculated with Lorentz line shapes differ substantially from those calculated with the correct line shape—the Voigt profile. Between 22 and 35 km the cooling obtained with the Voigt line shape (solid curve) becomes slightly less than that calculated with the Lorentz line shape. This region is referred to by *Dickinson* [1972] as the region of the Voigt dip. It is fortuitous that with this dip, Voigt lines give the same cooling as do Lorentz lines in combination with the Curtis-Godson approximation.

To account approximately for the change in line shape above 40 km, Ramanathan suggested that the line shape, either Lorentz or Doppler, that gives the largest cooling should be used. With this approximation he was able to obtain cooling rates for O_3 and CO_2 within 10% of those obtained by *Dickinson* [1973], who performed a line-by-line calculation employing the Voigt profile. Cooling rates obtained by using Ramanathan's approximation are indicated by the dashed curve in Figure 5. Below 41 km, Lorentz lines gave the largest cooling (heating below 27 km), while above, Doppler lines gave the largest cooling. The figure shows that cooling rates obtained for Doppler lines between 40 and 50 km are 0.2°K/d lower than those obtained for Voigt lines. Apparently, there is sufficient cooling from the Lorentzian wings of the Voigt lines that even at 50 km the cooling rate obtained for Doppler lines is 10% smaller than that obtained for Voigt lines. Nevertheless, above 40 km, Ramanathan's approximation gives cooling rates which are much closer to the actual rates than are those calculated for Lorentzian lines. In fact, Figure 5 shows that between 40 and 50 km, cooling rates obtained with Lorentz lines are barely within a factor of 2 of the actual rates.

To summarize, below 35 km we obtain reasonably accurate cooling rates and fluxes for the 9.6-μm band of ozone by using the Curtis-Godson approximation and the Lorentz line shape. Above 40 km we obtain cooling rates within 10–20% of the actual rates by using the line shape, Lorentz or Doppler, that gives the largest cooling. We should notice, however, that the Curtis-Godson and Lorentz line shape models give a cooling rate at 40 km which is only 0.3°K/d smaller than the actual rate. Since the total cooling due to H_2O, CO_2, and O_3 is about 5°K/d at this altitude, the error obtained by using these approximations is only 5% of the total cooling rate. Using the cool to space and Newtonian cooling approximations, we find that this cooling rate error would cause about a 3°K error in the temperature at 40 km. Such an error seems acceptably small for radiative-convective models. Thus models such as those developed by Manabe and his co-workers that are restricted to altitudes below 40 km are justified in using only Lorentz line shapes for ozone.

Now we consider the shapes of CO_2 lines. The CO_2 lines which contribute significantly to stratospheric cooling are considerably stronger than the O_3 lines. As a result they retain their Lorentzian shape at much lower pressures and therefore at much higher altitudes than do the O_3 lines. Listed in Table 3 are the vibration-rotation bands of CO_2 in the 15-μm region that significantly contribute to the long-wave cooling of the

TABLE 3. CO_2 Vibration-Rotation Bands in the 15-μm Region

Band Number	Isotope	Transition	Band Center, cm^{-1}	Band Strength at 300°K, $atm^{-1}\,cm^{-2}$	Cool to Space at 50 km, °K/d	Line Shape for Cool to Space at 50 km
1	$^{12}C^{16}O_2$	$00^00–01^10$	667.4	19.4	2.5	L
2	$^{12}C^{16}O_2$	$01^10–10^00$	720.8	5.0	0.40	L
3	$^{12}C^{16}O_2$	$01^10–02^00$	618.0	4.27	0.37	L
4	$^{12}C^{16}O_2$	$01^10–02^20$*	667.8	15.0	0.99	L
5	$^{12}C^{16}O_2$	$02^00–03^10$	647.1	1.0	0.23(0.18)	D(L)
6	$^{12}C^{16}O_2$	$02^20–03^30$*	668.2	0.85	0.26(0.24)	D(L)
7	$^{12}C^{16}O_2$	$02^20–03^10$*	597.3	0.14	0.14(0.096)	D(L)
8	$^{12}C^{16}O_2$	$02^20–11^10$*	741.7	0.12	0.13(0.089)	D(L)
9	$^{12}C^{16}O_2$	$02^00–11^10$	791.4	0.022	0.024	W
10	$^{12}C^{16}O_2$	$10^00–11^10$	688.7	0.3	0.15(0.099)	D(L)
11	$^{12}C^{16}O_2$	$10^00–03^10$	544.3	0.004	0.0046	W
12	$^{13}C^{16}O_2$	$00^00–01^10$	648.5	2.17	0.27(0.27)	D(L)
13	$^{12}C^{16}O^{18}O$	$00^00–01^10$*	662.3	0.78	0.25(0.23)	D(L)
14	$^{12}C^{16}O^{17}O$	$00^00–01^10$*	664.7	0.16	0.16(0.10)	D(L)

Line shapes are L, Lorentz; D, Doppler; and W, weak. Models used for the cool to space calculations are described in the text. The band strengths and band centers were obtained from *Drayson and Young* [1967].

*All lines present.

stratosphere. Also listed for each band is the cool to space contribution to the cooling rate at 50 km. At 50 km the cool to space term contributes more than half of the total cooling. These cooling rates were obtained for the U.S. Standard Atmosphere (1962) temperature profile and a CO_2 concentration of 330 ppm. The cooling rates for bands containing Lorentz lines were derived from the analytic expression for the equivalent width of the band obtained by J. A. Coakley (unpublished manuscript, 1978), while the cooling rates for bands containing Doppler lines were derived from the expressions for the equivalent width obtained by *Cess* [1973]. In these calculations the temperature dependencies of the band strengths were ignored for the first and second hot bands (those bands which have excited vibration levels for their lower level). As a result the cooling rates shown for the first hot bands (bands 2–4) are about 10% too high, while those for the second hot bands (bands 5–11) are about 20% too high. Provided the band did not contain mostly weak lines, the cooling rate was set equal to the larger of the two rates obtained for Lorentz and for Doppler shapes. If the band contains mostly weak lines, its contribution to the cooling is independent of line shape, and its contribution is in any event negligible.

As Table 3 shows, most of the cool to space contribution at 50 km comes from the fundamental band (band 1) and the first hot bands of $^{12}C^{16}O_2$. The strengths of these bands are sufficiently large that the lines which make up the band may be treated as strong Lorentz lines. The second hot bands and the isotopic bands, however, are considerably weaker, and therefore they contain many Doppler lines for the path to space at 50 km. Nevertheless, the total cooling due to all of the bands is 5.8°K/d, while the cooling obtained by assuming that all but the weak bands (bands 9 and 11) contain strong Lorentz lines is 5.5°K/d. Thus even at 50 km the use of the Lorentz profile for the line shapes in the 15-μm band of CO_2 results in errors which are less than 10% in the cooling rate. In conclusion, Lorentz lines will produce reasonably accurate stratospheric cooling rates for both CO_2 and O_3 in radiative-convective models provided that the model is restricted to altitudes below 40 km.

Detailed calculations of CO_2 cooling rates have been performed by *Drayson* [1967] and *Dickinson* [1973]. Dickinson shows explicitly the contribution of hot and isotopic bands, and his results are shown in Figure 6. Dickinson included all of the bands listed in Table 3 and also employed the Voigt line profile.

5. *Sensitivity of the Model*

Surface Temperature

As will be discussed in section G, radiative-convective models have frequently been used to obtain the first estimates of how the global average surface temperature might respond to changes in atmospheric composition. In radiative-convective models the surface temperature changes in response to the changes in the radiative energy received by the troposphere. The energy change of the troposphere, however, is constrained by the condition that the stratosphere must maintain a state of radiative equilibrium. As a result, changes in the stratosphere affect the radiative input into the troposphere and thereby affect the surface temperature. How changes in the stratosphere affect the troposphere is not always obvious. We there-

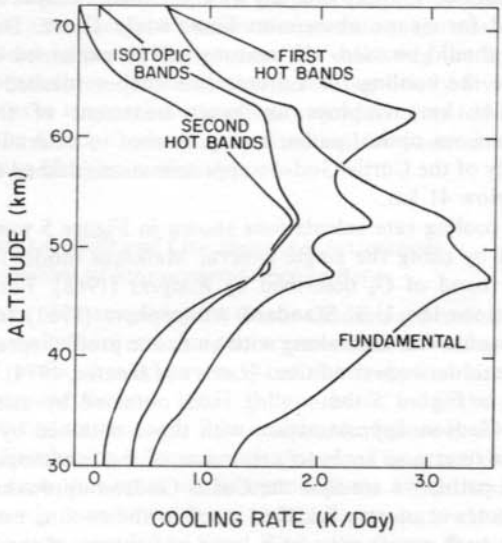

Fig. 6. Long-wave CO_2 cooling rates showing the contributions from fundamental, hot, and isotopic bands [after *Dickinson*, 1973].

fore offer the following simple model, which demonstrates how the surface temperature in a radiative-convective model responds to a perturbation.

For radiative-convective equilibrium the net outgoing long-wave radiative flux at the top of the atmosphere, F_{n0}, must equal the net solar radiative flux S_{n0}. Likewise, because the stratosphere is in radiative equilibrium, the net long-wave radiative flux at the base of the stratosphere, F_{n1}, must equal the net solar radiative flux into the troposphere, S_{n1}. For any perturbation the stratosphere and the atmosphere as a whole seek a new state of radiative equilibrium. Thus

$$dF_{n0} = dS_{n0} \tag{50}$$

and

$$dF_{n1} = dS_{n1} \tag{51}$$

Because we are concerned here with surface temperature changes, we will focus our attention on the radiative fluxes at the base of the stratosphere, level 1. From the equation of radiative transfer we see that F_{n0} and F_{n1} are given by

$$F_{n0} = F_1^+\tau + \epsilon \tag{52}$$

and

$$F_{n1} = F_1^+ - \epsilon \tag{53}$$

where τ is the transmissivity of the stratosphere for long-wave radiation, ϵ is the flux of radiation emitted by the stratosphere, and F_1^+ is the upward flux of long-wave radiation at the base of the stratosphere. In (52) and (53) the radiative flux emitted by the stratosphere upward to space is assumed to be equal to the flux emitted downward to the troposphere. This assumption, which is valid only for an isothermal stratosphere, should be reasonable, since the lower stratosphere, which contains 80–90% of the total mass of the stratosphere, is almost isothermal. Using (52) and (53), we also see that when the stratosphere is in radiative equilibrium, ϵ is given by

$$\epsilon = (S_{n0} - S_{n1} + F_1^+ - F_1^+\tau)/2 \tag{54}$$

With this condition, (51)–(54) may be combined to give the change in F_1^+ which is consistent with radiative-convective equilibrium:

$$dF_1^+ = dS_{n1} + \frac{dS_{n0} - dS_{n1}}{2} - \frac{F_1^+\, d\tau}{2} \tag{55}$$

Since the transmissivity of the stratosphere is close to unity, we have neglected $\frac{1}{2}(dF_1^+ - \tau\, dF_1^+)$ in (55) because it is small in comparison with dF_1^+. This approximation can be tested by comparing dF_{n0} with dF_{n1} for changes in tropospheric temperatures while stratospheric temperatures, and therefore ϵ, are held fixed.

Next we write dF_1^+, dS_{n1}, and dS_{n0} as

$$dF_1^+ = \frac{\partial F_1^+}{\partial g}dg + \frac{\partial F_1^+}{\partial T_s}dT_s \tag{56}$$

and

$$dS_{n0,1} = \frac{\partial S_{n0,1}}{\partial g}dg + \frac{\partial S_{n0,1}}{\partial T_s}dT_s \tag{57}$$

where dg denotes the change in external conditions or in atmospheric composition and dT_s denotes the change in the surface temperature. For a fixed relative humidity profile like that described by *Manabe and Wetherald* [1967] and for a constant tropospheric lapse rate, $\partial F_1^+/\partial T_s$ and $\partial S_{n1}/\partial T_s$ are almost constant. For our purposes we can assume that they are independent of temperature and atmospheric composition. Furthermore, we note that $\partial S_{n1}/\partial T_s$ and $\partial S_{n0}/\partial T_s$ are due to changes in the absorption of solar radiation by water vapor. Because most of this absorption takes place in the troposphere, $\partial S_{n0}/\partial T_s \simeq \partial S_{n1}/\partial T_s$.

Finally, from (52) and (53) we obtain

$$\frac{\partial F_1^+}{\partial g} - \frac{1}{2}\left(\frac{\partial F_1^+}{\partial g} - \frac{\tau\,\partial F_1^+}{\partial g}\right) = \frac{\partial F_{n1}}{\partial g} + \frac{1}{2}\left(\frac{\partial F_{n0}}{\partial g} - \frac{\partial F_{n1}}{\partial g}\right) - \frac{1}{2}\left(F_1^+\,\frac{\partial \tau}{\partial g}\right) \tag{58}$$

This result with (55), (56), and the assumptions that $\frac{1}{2}(dF_1^+ - \tau\, dF_1^+)$ can be neglected in comparison with dF_1^+ and the stratospheric transmissivity is insensitive to changes in atmospheric temperatures gives

$$\left(\frac{\partial F_1^+}{\partial T_s} - \frac{\partial S_{n1}}{\partial T_s}\right)\frac{dT_s}{dg} = \left(\frac{\partial S_{n1}}{\partial g} - \frac{\partial F_{n1}}{\partial g}\right) + \frac{1}{2}\left[\left(\frac{\partial S_{n0}}{\partial g} - \frac{\partial S_{n1}}{\partial g}\right) - \left(\frac{\partial F_{n0}}{\partial g} - \frac{\partial F_{n1}}{\partial g}\right)\right] \tag{59}$$

According to (59) the surface temperature of a radiative-convective model is affected primarily by two factors. The first factor, denoted by the term in parentheses on the right-hand side of (59), is the change of the net radiative flux into the troposphere caused by the perturbation when the atmospheric temperature is kept constant. The second factor, denoted by

TABLE 4. Effectiveness of (60) for Estimating the Surface Temperature Change of a Radiative-Convective Model

Perturbation	$\partial F_{n1}/\partial g$, W m^{-2}	$\partial F_{n0}/\partial g$, W m^{-2}	$\partial S_{n1}/\partial g$, W m^{-2}	$\partial S_{n0}/\partial g$, W m^{-2}	dT_s/dg (60), °K	dT_s/dg RC, °K
Double CO_2	−3.9	−1.6	0	0	1.2	1.6
Increase solar constant by 1%	0	0	2.3	2.4	1.1	1.0
Uniformly decrease O_3 by 30% between 12 and 40 km	0.2	0.5	1.0	−1.0	−0.2	−0.1
Uniformly decrease O_3 by 50% between 12 and 40 km	0.4	1.0	1.8	−1.7	−0.3	−0.2
Double stratospheric H_2O	−2.2	−0.1	−0.1	0.0	0.5	0.6

The flux changes and the radiative-convective model surface temperature changes were calculated by using the model developed by J. A. Coakley (unpublished manuscript, 1978). The flux changes were evaluated for the U.S. Standard Atmosphere (1962) temperature profile. Here dT/dg (60) is the estimate obtained from (60), and dT/dg RC is the change in the radiative-convective model surface temperature. For these estimates, $\partial F_1^+/\partial T_s = 2.4$ W m^{-2}, and $\partial S_{n1}/\partial T_s = 0.2$ W m^{-2}.

the term in brackets, is the change in the net radiative heating of the stratosphere. Because the stratosphere must maintain a state of radiative equilibrium, half of the change in its net heating is radiated to the troposphere; the other half is radiated to space. Equation (59) may be simplified to give

$$\frac{dT_s}{dg} = \frac{1}{2}\left(\frac{\partial S_{n0}}{\partial g} + \frac{\partial S_{n1}}{\partial g} - \frac{\partial F_{n0}}{\partial g} - \frac{\partial F_{n1}}{\partial g}\right) \cdot \left(\frac{\partial F_1^+}{\partial T_s} - \frac{\partial S_{n1}}{\partial T_s}\right)^{-1} \quad (60)$$

The effectiveness of this model is illustrated in Table 4. In the table we compare estimates of dT_s/dg obtained by using the radiative-convective model developed by J. A. Coakley (unpublished manuscript, 1978). We see that estimates of dT_s/dg obtained by using (60) agree well with the values of dT_s/dg obtained by using a radiative-convective model.

Equation (60) explains why simple energy balance models have been partially successful in simulating the behavior of radiative-convective models. In energy balance models [*Rasool and Schneider*, 1971; *Cess*, 1974; *Pollack et al.*, 1976], instead of computing the radiative equilibrium temperature profile of the stratosphere the temperature profile is specified and usually held fixed. The temperature profile of the model atmosphere is therefore linked to the surface temperature via the constant tropospheric lapse rate. The equilibrium surface temperature of the model is that for which the net long-wave radiative flux cancels the net solar radiative flux at the top of the model atmosphere. To maintain this state of radiative equilibrium, the change in the equilibrium surface temperature for a particular perturbation is that for which the change in the net long-wave radiative flux cancels the change in the net solar radiative flux. The change in the surface temperature of an energy balance model is therefore given by

$$\frac{dT_s}{dg} = \left(\frac{\partial S_{n0}}{\partial g} - \frac{\partial F_{n0}}{\partial g}\right)\left(\frac{\partial F_{n0}}{\partial T_s} - \frac{\partial S_{n0}}{\partial T_s}\right)^{-1} \quad (61)$$

We note that because of the transparency of the stratosphere, $\partial F_{n0}/\partial T_s \simeq \partial F_1^+/\partial T_s$ for fixed stratospheric temperatures and therefore that (60) and (61) are practically equivalent when $\partial S_{n0}/\partial g \simeq \partial S_{n1}/\partial g$ and $\partial F_{n0}/\partial g \simeq \partial F_{n1}/\partial g$. This occurs, for example, as is shown in Table 4, when the perturbation is a change in the solar constant. Cess and Pollack et al. note that their energy balance models predict surface temperature changes in response to solar constant changes that are rather similar to those obtained by *Manabe and Wetherald* [1967].

The condition for the equivalence of (60) and (61) will also hold when the perturbation is confined to the troposphere. For example, upon removing tropospheric clouds from their model, *Manabe and Wetherald* [1967] found $dS_{n0}/dg = 71$ W m^{-2} and $dF_{n0}/dg = 25$ W m^{-2}. For their model

$$\frac{\partial F_{n0}}{\partial T_s} - \frac{\partial S_{n0}}{\partial T_s} = 2.2 \text{ W m}^{-2}$$

Using (61), we obtain $dT_s/dg = 21$°K, in good agreement with the 19.4°K change obtained with their radiative-convective model.

Clearly, (61) will not be equivalent to (60) when the perturbation causes changes in the stratosphere. As is shown by the results in Table 4, energy balance models that are based on (61) will give unreliable estimates of dT_s/dg for CO_2, O_3, and stratospheric H_2O perturbations. As will be discussed in section G1, by disregarding the condition of radiative equilibrium for the stratosphere Rasool and Schneider obtained for a doubling of CO_2 a surface temperature change which was substantially smaller than that which would have been obtained if the conditions of radiative-convective equilibrium had been satisfied.

6. *Feedback Mechanisms*

Here we will describe the influence of the various feedbacks on the sensitivity of the model. A useful measure of the model sensitivity is the sensitivity of the surface temperature to a change in the solar constant defined by the sensitivity parameter β [*Schneider and Dickinson*, 1974]:

$$\beta = S_0 (dT_s/dS) \quad (62)$$

where S is the solar constant and S_0 is the present value of S with $S_0 = 1360$ W m^{-2}. The parameter β can be derived from the global energy equation

$$(S/4)(1 - \alpha_p) = F \quad (63)$$

where α_p is the planetary albedo and F is the outgoing long-wave flux at the top of the atmosphere. From (63) we obtain

$$\beta = S_0 \frac{dT_s}{dS} = \frac{F}{(dF/dT_s) + (S_0/4)(d\alpha_p/dT_s)} \quad (64)$$

Note that (64) is analogous to (61) in that (64) neglects the effects on dT_s due to changes in stratospheric temperatures. Following *Cess* [1976], we can write F and α_p as

$$F = C_1 - A_c C_2$$
$$\alpha_p = (1 - A_c)\alpha_S + A_c \alpha_c \quad (65)$$

where A_c is the fractional cloud cover, C_1 is the clear sky contribution to F, C_2 is the reduction in F due to the presence of clouds, α_s is the albedo of the clear sky region of the earth-atmosphere system, and α_c is the albedo of the cloud-covered region. From (65) we obtain

$$\frac{dF}{dT_s} = \frac{\partial F}{\partial T_s} + \frac{\partial F}{\partial A_c}\frac{dA_c}{dT_s}$$
$$\frac{d\alpha_p}{dT_s} = \frac{\partial \alpha_p}{\partial T_s} + \frac{\partial \alpha_p}{\partial A_c}\frac{dA_c}{dT_s} \quad (66)$$

The second terms on the right-hand sides of (66) arise because of the possible interaction between T_s and cloud amount. This interaction has been neglected in radiative-convective models; i.e., the models assume $(dA_c/dT_s) = 0$. The term C_1 in (65) depends on T_s, the lapse rate, the surface relative humidity, and the vertical distribution of relative humidity. The cloud correction term C_2 depends on the preceding parameters and, in addition, depends on the cloud top temperature. All of these parameters in turn are assumed to depend on T_s, and this mutual dependence determines the value of $\partial F/\partial T_s$ and hence β. A contribution to $\partial \alpha_p/\partial T_s$ arises because of the coupling between T_s, relative humidity, and H_2O solar absorption. Other possible contributions due to coupling between T_s and ice and snow cover (among several possibilities) are not included in the model.

The quantitative effect of various feedbacks is shown in Table 5. The value of β indicates the change in T_s for 1% change in the solar constant. For example, $\beta = 65$°K implies a change in T_s of 0.65°K for 1% change in the solar constant. By comparing rows 1 and 2 we see that fixing the relative humidity instead of the absolute humidity in the model nearly doubles

TABLE 5. Comparison of Climate Sensitivity Parameters for Several Radiative-Convective Models

β, °K				
FAH and FCA	FRH and FCA	FRH and FCT	VRH* and FCA	Reference
65	129			*Manabe and Wetherald* [1967]
	125	231		*Cess* [1974]
	121	197		*Ramanathan* [1976]
		160		*Wang et al.* [1976]
			165	*Cess* [1976]

All of the models neglect the cloud amount feedback. FAH is fixed absolute humidity, FRH is fixed relative humidity, FCA is fixed cloud altitude, FCT is fixed cloud top temperature, and VRH is variable relative humidity distribution. For the VRH and FCA model, $\Omega = 1 - 0.03(T_s - 288)$ (see section E*1c*, equation (49) for the definition of Ω.

the sensitivity of the model. By comparing the second and third columns in Table 5 we see that the FCT model is significantly more sensitive (by a factor of 1.6–2) than the FCA model. The FCT and FCA models are discussed by *Cess* [1974]. A comparison of the second and fourth columns indicates the effect of varying the atmospheric relative humidity distribution with T_s.

Most of the contribution to β comes from the infrared sensitivity parameter dF/dT_s (W m^{-2} °K^{-1}) in the denominator of (64). For example, for the model with fixed relative humidity (FRH) and FCA,

$$dF/dT_s = 2.25$$
$$(S_0/4)(d\alpha_p/dT_s) = -0.24 \tag{67}$$

The values in (67) are obtained from *Ramanathan* [1976]. The reason for the larger sensitivity of the FCT model can be seen by comparing the values of dF/dT_s given by *Ramanathan et al.* [1976],

FCA and FRH

$$dF/dT_s = 2.16 + A_c 0.19 \tag{68a}$$

FCT and FRH

$$dF/dT_s = 2.16 - A_c 1.75 \tag{68b}$$

The results shown in Table 4 clearly illustrate the large uncertainty in the model results introduced by the model assumptions concerning the prescription of H_2O and cloud top in the model. Of these models the fixed absolute humidity (FAH) model is considered to be unrealistic, since, as was discussed by *Manabe and Wetherald* [1967], the atmosphere tends to conserve its relative humidity instead of absolute humidity with changes in T_s. Accordingly, all of the radiative-convective models adopt the FRH model. In regard to the prescription of the cloud top in the model, there are no convincing theoretical justifications for preferring the FCA model over the FCT model.

In addition to those discussed thus far, there are other potentially important feedbacks which, in principle, can be included in the radiative-convective model. These additional feedbacks, which were investigated by *Coakley* [1977*b*], arise because of the dependence of F on the tropospheric lapse rate Γ and on the surface relative humidity RH^*.

7. *Role of H_2O, CO_2, O_3, and Clouds*

Manabe and Strickler [1964] and *Manabe and Wetherald* [1967] have performed computations to estimate the individual contributions of H_2O, CO_2, O_3, and clouds on the surface temperature. These calculations show that the gases H_2O, CO_2, and O_3 have a net warming effect on T_s, while clouds have a net cooling effect on T_s.

Manabe and Strickler's model results indicate that CO_2 warms the surface by about 10°K and O_3 warms the surface by about 1°K. These calculations were performed with an FAH model for clear sky conditions. Since the sensitivity of the FAH model is roughly half that of the FRH model, it is possible that the actual warming effects of CO_2 and O_3 are larger than those estimated by Manabe and Strickler. The warming effect of gaseous H_2O has not been estimated by any of the models. Most of the effect of H_2O on T_s arises because of its opacity in the long-wave spectral region. Table 6 shows the relative contributions of H_2O, CO_2, and O_3 to reducing the outgoing long-wave flux, from which it is seen that the long-wave effect of H_2O is significantly larger than the effects of CO_2 and O_3.

Clouds have two competing opposite effects on T_s. (1) Clouds reflect a large portion of the incident solar radiation. On a globally averaged basis the albedo of the cloud-covered portion of the earth is 0.45–0.5, while the albedo of the cloudless part is 0.14–0.18. Hence the albedo modification tends to cool the surface. (2) Most clouds are opaque to long-wave radiation, and hence they substantially reduce the long-wave radiation escaping to space. Denoting the net effect of clouds by σ, we can express σ by

$$\sigma = A_c C_2 - (S_0/4)A_c(\alpha_c - \alpha_s) \tag{69}$$

where we have made use of (63) and (65) to obtain (69). On the right-hand side the first term is the long-wave modification due to clouds, the second term denotes the albedo modification due to clouds, and σ is the net change in the energy absorbed by the earth-atmosphere system. Clouds have a net cooling (warming) if σ is negative (positive). Equation (69) is derived for a single cloud and can be easily extended for multiple cloud layers.

The model calculations of *Manabe and Wetherald* [1967] and *Schneider* [1972] indicate that σ is negative and large. Manabe and Wetherald calculated T_s in their model with and without the three-level clouds and estimated that T_s is 19°K cooler with clouds than without clouds. Schneider calculates $\sigma \approx -27$ W m^{-2}, which corresponds to a surface cooling of about 13°K. More recently, *Ellis* [1977] has estimated σ from satellite measurements. By comparing clear and cloudy sky

TABLE 6. Relative Contribution of H_2O, CO_2, and O_3 to Outgoing Long-Wave Flux F

Gases Considered in Calculation	F, W m^{-2}	$\delta F = [F(1) - F/F(1)] \times 100$
H_2O, CO_2, O_3	227.3	
H_2O, O_3	247.5	−9
H_2O, CO_2	232.5	−2
CO_2, O_3	284.5	−25

The calculations were performed with *Ramanathan*'s [1976] model for average cloudiness conditions, cloud amount of 0.45, cloud top altitude of 6.25 km, and standard atmosphere temperature distribution. The assumed O_3 and H_2O relative humidity distributions are given in the same reference. Values of δF are the net percent changes in F due to the gas omitted from the calculation.

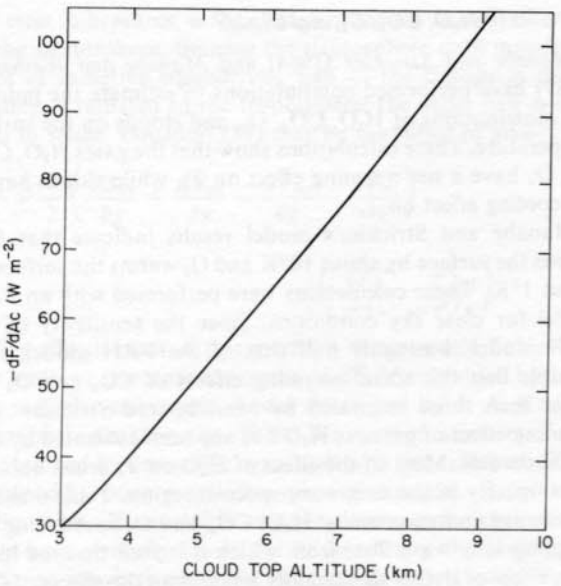

Fig. 7. Long-wave modification effect due to clouds as a function of cloud altitude. F is the outgoing long-wave flux at the top of the atmosphere, and A_c is the fractional cloud amount.

outgoing fluxes and albedos for annual and global average conditions, Ellis obtained $\sigma \approx -21$ W m^{-2}. Thus the model calculations and observations indicate that clouds have a net cooling effect on the global climate. The net cooling effect is the integrated effect of all the multilevel clouds. *Manabe and Wetherald* [1967] examined how the net effect depends on cloud altitude and obtained the following results:

Low clouds

$$dT_s/dA_c = -82°\text{K} \tag{70a}$$

Middle clouds

$$dT_s/dA_c = -39°\text{K} \tag{70b}$$

High clouds

$$dT_s/dA_c = +17°\text{K} \tag{70c}$$

The primary reason for the sign change of dT_s/dA_c from low to high clouds is the strong dependence of the long-wave radiative flux on cloud altitude. This dependence is clearly illustrated in Figure 7, where the parameter C_2 is plotted as a function of cloud top altitude. Since the temperature decreases with increasing altitude, high clouds emit less radiation to space than do low clouds. As a result a given amount of high clouds causes a larger change in the outgoing long-wave flux than that caused by the same amount of low clouds.

As was shown by *Schneider* [1972], both the albedo and the long-wave modifications due to clouds are strong functions of latitude and season. Since radiative-convective models ignore these variations, we should consider the results presented here concerning cloud effects as being only tentative.

G. Studies of Climate Change

Several radiative-convective model studies have been performed to assess the changes in T_s that may result from perturbations in the optically active constituents in the atmosphere—aerosols, CO_2, H_2O, O_3, fluorocarbons, chlorocarbons, N_2O, NO_2, and CH_4. The motivation for these studies stems from the possibility that appreciable perturbations in the ambient concentrations of these compounds may arise because of anthropogenic sources. To mention a few examples, several studies have indicated that continued burning of fossil fuels will double that CO_2 concentration in the atmosphere by the middle of the twentieth century. In support of their argument these studies point out that the steady increase of CO_2 from the preindustrial value of about 295 ppm (by volume) in 1860 to the value of 330 ppm in 1974 is due to the burning of fossil fuels (see the report of *Baes et al.* [1976] for a summary of the projected increase of CO_2 in the atmosphere). More recently, several studies have raised the possibility that nitrogen oxides injected by high-altitude supersonic transports (SST), fertilizers used in agriculture, and fluorocarbons used as refrigerants and as propellants in aerosol cans can significantly perturb the ozone concentrations in the stratosphere. Radiative-convective model results have provided an invaluable first estimate for the possible climatic effects of such perturbations in the optically active atmospheric constituents. We will summarize these results here.

In judging the importance of these results it should be remembered that they represent only the sensitivity of the model climate to perturbations in the atmospheric constituents and that the sensitivity of the model may not reflect the climate sensitivity of the actual earth-atmosphere system. For the CO_2-climate problem, however, the increase in T_s due to an increase in CO_2 computed by the radiative-convective model is within 20% of the increase in T_s computed by a three-dimensional general circulation climate model [see *Manabe and Wetherald*, 1975]. Hence it is felt that radiative-convective model results are at least indicative of the potential sensitivity of our climate.

1. *Increase in CO_2*

The effect of increasing CO_2 on the global surface temperature has been examined in several studies, and the results of these studies have been summarized by *Schneider* [1975]. There is qualitative agreement between all of these studies in that they show that increasing CO_2 will cause an increase in T_s. The increase in T_s arises from two effects: (1) increase in the opacity of the atmosphere in the long-wave region and (2) increase in the solar absorption by the near-infrared bands of CO_2. Most (about 87%) of the contribution to the increase in T_s arises from the enhancement in the long-wave opacity. The long-wave and solar bands of CO_2 are listed in Table 7.

Manabe and Wetherald [1967] performed the first radiative-

TABLE 7. Long-Wave and Solar Bands of CO_2

Spectral Region, μm	Band Type
	Long-Wave Bands
12–18	fundamental, isotopic, and hot bands (see Table 3 for a listing of the most important bands)
10	two hot bands
7.6	fundamental band
	Solar Bands
4.3	fundamental, isotopic, and hot bands (see *Dickinson* [1972] for a listing of the number of bands in each spectral region)
2.7	
2.0	
1.6	
1.4	
1.2	

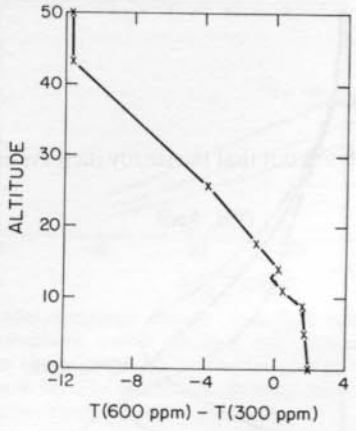

Fig. 8. Radiative-convective model results for the change in atmospheric temperature due to a doubling of CO_2 [after *Manabe*, 1971].

convective model calculations for the increase in T_s, ΔT_s, due to a doubling of CO_2 from 300 to 600 ppm. They obtained $\Delta T_s = 2.4°K$. *Manabe* [1971] subsequently improved the treatment of long-wave radiation in their model and obtained a value of $\Delta T_s = 1.95°K$ with the improved model. The change in the surface and atmospheric temperature computed by Manabe's model is shown in Figure 8. It is seen that increasing CO_2 concentration has opposite effects on the temperatures of the troposphere and stratosphere. The cooling of the stratosphere results from an increase in long-wave radiation emitted to space by the CO_2 in the stratosphere. The warming of the surface and troposphere results primarily from an enhanced absorption of the surface long-wave radiation by the tropospheric CO_2. An additional effect which causes the tropospheric warming is an effective increase in the downward radiation emitted by stratospheric CO_2. *Schneider* [1975] has shown that this effective increase in the downward long-wave radiation results from two competing opposite effects. (1) The decrease in stratospheric temperature causes a reduction in the downward radiation emitted by the stratosphere. (2) The increase in CO_2 concentration causes an increase in the downward emission by the long-wave bands of CO_2. The second effect dominates the first effect, the result being a net increase in the downward radiation emitted by the stratosphere. *Schneider* [1975] estimates that this increase in the long-wave energy input into the troposphere contributes about 0.5°K to the computed increase in T_s. *Rasool and Schneider* [1971] neglected the above mentioned stratospheric contribution to ΔT_s and obtained a substantially lower value for ΔT_s.

Schneider [1975] concludes that the models of *Manabe* [1971], *Ramanathan* [1975*a*], and *Schneider* [1975] provide the most reliable estimates for ΔT_s, which estimate 1.9, 1.5, and 1.45°K, respectively, for a doubling of the CO_2 concentration. All three models neglect the 10-μm and 7.6-μm bands of CO_2 (see Table 7). More recently, *Augustsson and Ramanathan* [1977] adopted the radiative-convective model of *Ramanathan* [1976], reevaluated ΔT_s after including all of the CO_2 bands listed in Table 7, and estimated $\Delta T_s = 1.98°K$. The contributions from the individual CO_2 bands to the total value of 1.98°K are as follows: 12- to 18-μm bands, 1.61°K; 10- and 7.6-μm bands, 0.12°K; and solar bands of CO_2 and H_2O, 0.25°K. The solar bands of H_2O contribute to ΔT_s because of the previously mentioned coupling between T_s, H_2O amount, and solar absorption by H_2O.

Augustsson and Ramanathan explained that the models of *Ramanathan* [1975*a*] and *Schneider* [1975] yielded lower values for ΔT_s because of the neglect of four weak bands of CO_2 in the 12- to 18-μm region (bands 7–9 and 11 in Table 3) which contribute about 0.33°K to ΔT_s. By adding 0.33°K to the results of *Ramanathan* [1975*a*] and *Schneider* [1975] these two models yield $\Delta T_s \approx 1.83°K$, which agrees with *Manabe*'s [1971] value of 1.9°K. All of the results discussed above were obtained with the fixed cloud altitude and fixed relative humidity version of the model. Results for other versions, such as fixed cloud temperature and variable relative humidity, are presented by Augustsson and Ramanathan.

2. *Increase in Aerosols*

How the global mean surface temperature might respond to an increase in atmospheric aerosols is far more difficult to estimate than how it might respond to an increase in CO_2. The effect of aerosols on the long-wave and solar radiative fluxes depends, of course, on both aerosol concentration and optical properties. Both concentrations and optical properties are highly variable in space and in time, and as a result of this variability, neither concentrations nor optical properties are well known. Furthermore, unlike the increase in CO_2, which appears to be uniform over the globe, increases in atmospheric aerosols are likely to be regional, the regions of increase being fairly well determined by aerosol sources and prevailing winds. Since by design a radiative-convective model is a global average model, we cannot expect to use it to obtain realistic estimates of temperature changes caused by localized increases in aerosols. Nevertheless, radiative-convective calculations can be used to clarify our understanding of how a particular aerosol might influence the atmospheric radiation and how this perturbation in atmospheric radiation might be reflected in the atmospheric temperature profile if the other sources of energy (such as advection of energy from regions outside the region being studied) could be ignored. In view of these limitations we tend to emphasize the qualitative rather than the quantitative results of radiative-convective model studies of increases in atmospheric aerosols.

Increases of tropospheric aerosols have been studied with radiative-convective models by *Reck* [1974*a*, 1974*b*, 1975] and by *Wang and Domoto* [1974]. We should expect that tropospheric aerosols, like the tropospheric clouds in Manabe and Wetherald's model (cf. section F5), would have only a small influence on the stratosphere, and therefore we should be able to estimate the change in the surface temperature from

$$\frac{dT_s}{dq} = -\frac{dF/dq + (S_0/4)(d\alpha_p/dq)}{dF/dT_s + (S_0/4)(d\alpha_p/dT_s)} \tag{71}$$

where q is a measure of the column amount of aerosol.

Aerosols, like any atmospheric constituent, cause a reduction in the long-wave radiative flux at the top of the atmosphere. Thus an increase in q causes a decrease in F, and therefore the sign of dF/dq is negative. The planetary albedo, on the other hand, either increases or decreases with an increase in aerosols. The sign of $d\alpha_p/dq$ depends on how much solar radiation the aerosol absorbs, how much it scatters, and also on the planetary albedo prior to the addition of the aerosols [*Chýlek and Coakley*, 1974]. Aerosols which absorb much solar radiation but scatter little are likely to cause a decrease in the planetary albedo, while those which absorb little but scatter much are likely to cause an increase. Also, provided the aerosol absorbs some solar radiation, it tends to cause a decrease in the planetary albedo when the planetary

albedo is high; provided the aerosol scatters some solar radiation, it tends to cause an increase in the planetary albedo when the planetary albedo is low.

The aerosols studied so far in radiative-convective models consist of spherical particles with radii mostly between 0.1 and 1 μm. Because of their sizes these particles interact more strongly with solar radiation, which includes wavelengths comparable to the particle radii, than with long-wave radiation, which contains wavelengths several times the particle radii. As a result, dF/dq has usually been found to be much smaller than $(S_0/4)(d\alpha_p/dq)$ [*Rasool and Schneider,* 1971; *Wang and Domoto,* 1974], and therefore the sign of the surface temperature change is mostly determined by the sign of $d\alpha_p/dq$.

Some of the results of the radiative-convective model calculations are in agreement with the above analysis. Both *Wang and Domoto* [1974] and *Reck* [1974*b*] find a critical surface albedo (and therefore a critical planetary albedo) such that an increase in aerosols causes surface cooling (warming) when the surface albedo is smaller (larger) than the critical value.

Other results do not, however, agree with the above analysis. Reck uses a two-stream approximation to compute aerosol reflectivities and transmissivities, and these are then used in a parametric scheme for radiative transfer like the scheme described in section C2. She finds that in order for the aerosol to cause surface warming it must absorb substantially more solar radiation than would be predicted by the two-stream approximation for the change in planetary albedo [*Reck,* 1974*b*; *Chýlek and Coakley,* 1974]. The higher absorption is probably needed because Reck has neglected the aerosol absorption of solar radiation that has been reflected by the surface and clouds. *Wang and Domoto* [1974], on the other hand, find that when they add a small concentration of aerosols to an otherwise clear atmosphere, $-[dF/dq + (S_0/4)(d\alpha_p/dq)] > 0$, yet their model predicts a -2°K change in surface temperature. This result is impossible to reconcile with the above analysis. Wang and Domoto also find that in the lower troposphere, aerosols contribute to long-wave warming. This result disagrees with the long-wave cooling obtained by others [*Ackerman et al.,* 1976; *Fiocco et al.,* 1976]. The reasons for such discrepancies are unknown. Perhaps further radiative-convective model studies of the effects of tropospheric aerosols may resolve these conflicts.

Recently, *Hansen et al.* [1978] studied the radiative-convective model temperature change caused by an increase in stratospheric aerosols. Previously, such temperature changes had been studied only with energy balance models [*Harshvardhan and Cess,* 1976; *Pollack et al.,* 1976; *Coakley and Grams,* 1976]. All of these energy balance studies suggested that the surface would probably cool with an increase in stratospheric aerosols, but some studies indicated that depending on the optical properties of the aerosols the stratosphere would warm with the increase [*Harshvardhan and Cess,* 1976; *Fiocco et al.,* 1976], while others indicated that cooling could also occur [*Pollack et al.,* 1976; *Coakley and Grams,* 1976].

Hansen et al. used their radiative-convective model to study the temperature changes caused by the large increase in stratospheric aerosols after the explosive eruption of Mount Agung in 1963. For this increase they obtained a slight surface cooling and a substantial stratospheric warming. By setting ocean and atmospheric meridional energy transports equal to observed values they were able to apply modified conditions of radiative-convective equilibrium to the tropical atmosphere. The temperature changes obtained by Hansen et al. agree remarkably well with the temperature changes observed after the eruption [*Newell,* 1971; *Newell and Weare,* 1976]. Of course, because of the uncertainties in aerosol sizes and optical properties and in the validity of the model assumptions, there is considerable uncertainty in the calculated temperature changes. This uncertainty combined with the noisiness of the climatic record precludes firm conclusions concerning the agreement between the model results and the observations. Nevertheless, the good agreement is rather satisfying.

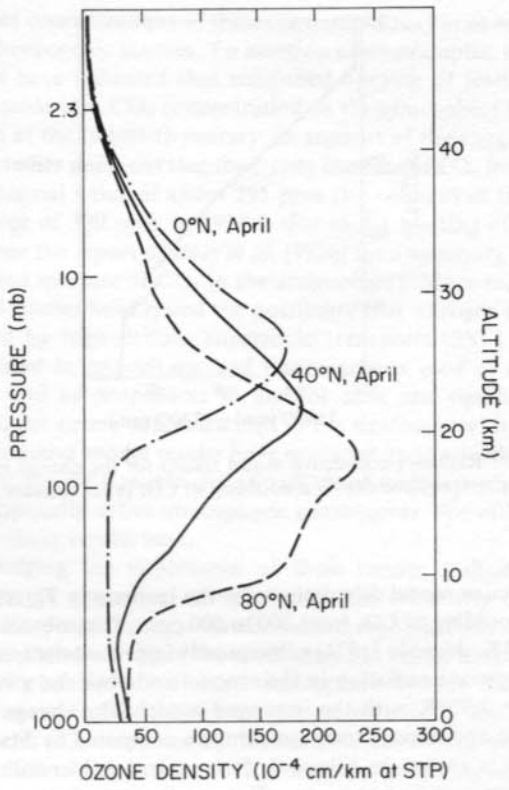

Fig. 9. Observed ozone density profiles for low, middle, and high latitudes (reprinted with permission of *Manabe and Wetherald* [1967] and the American Meteorological Society).

3. *Perturbations in O_3 and NO_2*

The influence of ozone on the global energy balance was first examined by *Manabe and Wetherald* [1967]. Manabe and Wetherald computed T_s for three different distributions of ozone representative of spring conditions for low, middle, and high latitudes. The three distributions of O_3 adopted by these authors are shown in Figure 9, and their results for T_s are shown in Table 8. As is seen from this table, decreasing the total O_3 amount causes the surface to cool. The estimated changes in T_s were partly caused by the differences in the vertical distribution of O_3 between the three profiles. *Ramanathan et al.* [1976] performed a more detailed analysis of the O_3-T_s relationship and concluded that T_s is equally sensitive to

TABLE 8. Global Surface Temperatures for the Three Ozone Distributions Shown in Figure 9

O_3 Distribution	Total O_3 Amount, cm, STP	T_s, °K
0°N, April	0.26	287.9
40°N, April	0.351	288.8
80°N, April	0.435	290.3

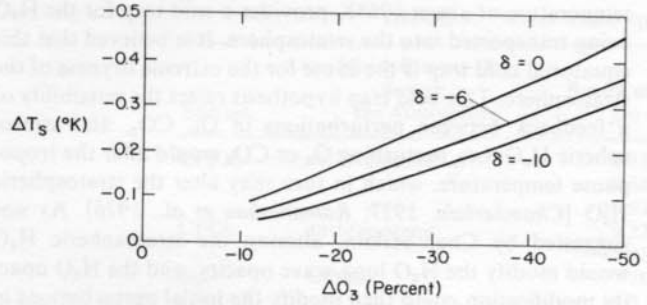

Fig. 10*a*. Model-computed change in surface temperature as a function of stratospheric ozone decrease and nitrogen dioxide increase: δ denotes the ratio of the fractional change in NO_2 to the fractional change in O_3. The results are obtained with the fixed cloud altitude model [after *Ramanathan et al.*, 1976].

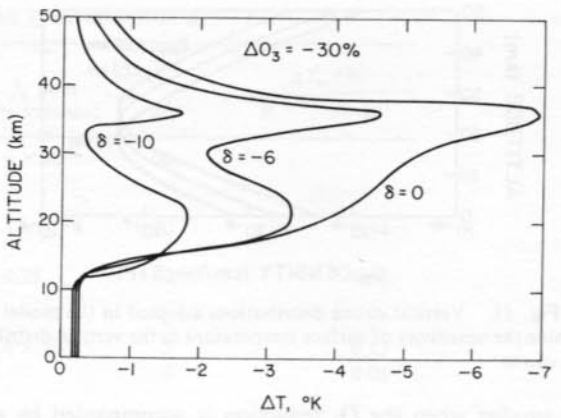

Fig. 10*c*. Model-computed change in atmospheric temperature for a 30% uniform reduction in stratospheric ozone and for various values of δ.

both the total ozone amount and the vertical O_3 distribution. We will summarize the results of Ramanathan et al. (hereafter referred to by R) below.

The R analyses considered three types of O_3 perturbations: (1) uniform reduction in stratospheric O_3, (2) uniform reduction in O_3 accompanied by a simultaneous increase in NO_2, and (3) change in the vertical O_3 distribution. The motivation for considering case (2) is to examine the type of O_3 reduction that may result from a potential fleet of SST's. It was first indicated by *Johnston* [1971] and *Crutzen* [1972] that nitrogen oxides from the effluents of SST engines may cause a net reduction in stratospheric O_3. These analyses further indicated that the reduction in O_3 will be accompanied by an increase in stratospheric NO_2 concentration. NO_2 has solar absorption bands in the 0.12- to 0.7-μm region, and hence the increase in NO_2 solar absorption due to an increase in NO_2 would modify the effect of the O_3 reduction on T_s.

The results of case (1) and case (2) for T_s and atmospheric temperatures are shown in Figures 10*a*–10*c*. The parameters ΔO_3 and δ are defined as

$$\Delta O_3 = \frac{O_3^1 - O_3^0}{O_3^0} \times 100 \tag{72}$$

$$\delta = \Delta NO_2/\Delta O_3 \tag{73}$$

and

$$\Delta NO_2 = \frac{NO_2^1 - NO_2^0}{NO_2^0} \times 100 \tag{74}$$

where O_3 and NO_2 are the densities of O_3 and NO_2, respectively, and O_3^1 and O_3^0 denote the density of O_3 in the perturbed and ambient atmosphere, respectively. The perturbations were considered to be uniform in the stratosphere, i.e., ΔO_3 = const above 12 km, and $\Delta O_3 = 0$ below 12 km such that ΔO_3 and ΔNO_2 also denote the percent perturbation in the total amount of O_3 and NO_2 in the stratosphere and δ denotes the ratio of the percent change between NO_2 and O_3. In Figure 10*a* the $\delta = 0$ curve represents case (1), and the $\delta = -6$ and $\delta = -10$ curves represent case (2). Restricting our attention to the $\delta = 0$ curve, which represents a reduction in O_3 without a perturbation in NO_2, we see that reducing O_3 cools the surface, in qualitative agreement with Manabe and Wetherald's results. The cooling of the surface results from two competing effects. (1) Reducing stratospheric O_3 reduces the stratospheric absorption of solar radiation by O_3, which results in an increase in the direct solar radiation reaching the troposphere. A fraction (about 70%) of this increased solar radiation is absorbed by the troposphere and surface. This increased absorption of solar radiation by the surface tends to warm the surface and troposphere. (2) The second effect tends to cool the troposphere and surface. This cooling is due to the reduction in the downward long-wave flux emitted by the stratosphere into the troposphere. The reduction in the downward long-wave flux is due to the cooling of the stratosphere which accompanies the reduction in O_3. The surface cooling due to O_3 reduction can also be understood on the basis of the numbers given in Table 4 and the discussions in section G5 following (60). The magnitude of the stratospheric cooling is shown in Figure 10*c* for $\Delta O_3 = -30\%$. The cooling above 25 km is due to the reduction in solar absorption by O_3, while the cooling between 12 and 15 km is primarily due to the reduction in absorption of the tropospheric long-wave radiation by the 9.6-μm band of O_3. As is evident from Figure 10*a*, the cooling of the surface by the second effect dominates the warming by the first effect.

The effect of a simultaneous increase in NO_2 can be seen by comparing the $\delta = -6$ and $\delta = -10$ curves with the $\delta = 0$ curve in Figures 10*a* and 10*c*. Increasing NO_2 partially compensates for the decrease in T_s due to the reduction in O_3. The magnitude of the stratospheric cooling is smaller when the reduction in O_3 is accompanied by an increase in NO_2 (compare the three curves in Figure 10*c*), because the increased solar absorption by NO_2 partially compensates for the decreased solar absorption by O_3. Consequently, the reduction in the stratospheric downward long-wave flux into the troposphere is smaller for values of $-\delta > 0$, and hence, as is shown in Figure 10*a*, $-\Delta T_s$

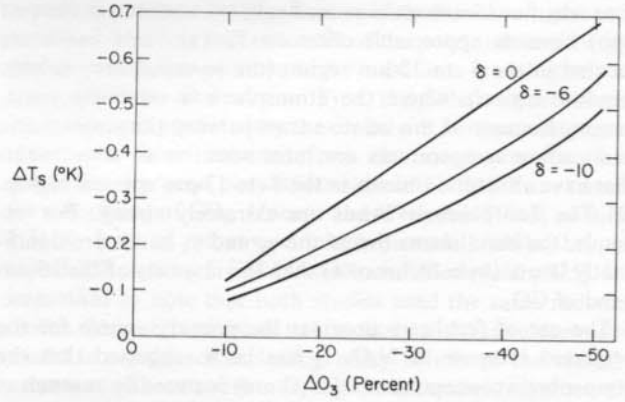

Fig. 10*b*. Same as Figure 10*a* but for the fixed cloud temperature model.

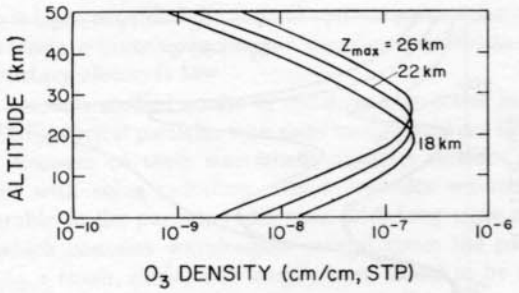

Fig. 11. Vertical ozone distributions adopted in the model to examine the sensitivity of surface temperature to the vertical distribution of ozone.

is smaller when the O_3 reduction is accompanied by an increase in NO_2.

The ΔT_s results for the FCT model are shown in Figure 10*b*. As is expected, ΔT_s for the FCT model is a factor of about 1.6 larger than ΔT_s for the FCA model. The sensitivity of T_s to the vertical O_3 distribution was analyzed in the R model by computing T_s for the three O_3 distributions shown in Figure 11, where z_{max} refers to the altitude at which the O_3 density is maximum. The total ozone amount is the same for all three curves. The computed values of T_s are 288.66, 288.00, and 287.56 for the three distributions marked z_{max} = 18, 22, and 26 km, respectively; i.e., the surface cools as z_{max} is increased. The dependence of T_s on z_{max} arises from the dependence of the O_3 9.6-μm band opacity on z_{max}. The 9.6-μm band of O_3 is a vibration-rotation band of pressure-broadened lines, and hence its opacity depends on the product of the O_3 density and the atmospheric pressure P. If τ_0 is the total opacity of the 9.6-μm band in the atmosphere, then

$$\tau_0 \propto \int_0^\infty O_3(z)P(z)\,dz \tag{75}$$

where z is the altitude. From Figure 11 we see that as z_{max} is increased, the O_3 distribution is shifted vertically upward such that more O_3 is located at lower pressures, and from the equation for τ_0 it follows that τ_0 decreases as z_{max} increases. Consequently, the greenhouse effect due to O_3 decreases as z_{max} is increased, resulting in the negative correlation between z_{max} and T_s. Increasing z_{max} by 4 km from 22 km cools T_s by 0.44°K, and comparing this value with the ΔT_s values shown in Figure 10, we see that increasing z_{max} by 4 km causes as much of an effect on T_s as that caused by a 50% reduction in stratospheric O_3. These results indicate that from the climatic viewpoint, perturbations in the vertical distribution of O_3 may be as important as perturbations in the total O_3 amount.

Radiative-convective model estimates of ΔT_s for a reduction in O_3 have also been computed by *Wang et al.* [1976] and J. A. Coakley (unpublished manuscript, 1978). These studies also predict a decrease in T_s for a uniform reduction in O_3, but the magnitude of ΔT_s is substantially different. For a 30% uniform reduction in stratospheric O_3, Coakley estimates (as is shown in Table 4) $\Delta T_s = -0.1$°K for the FCA version of his model, while $\Delta T_s = -0.26$°K for the R model. For the FCA model, Wang et al. estimate $\Delta T_s = -0.34$ for a 25% reduction in total ozone. A direct comparison between the results of Wang et al. and those of R is not possible, since Wang et al. reduce O_3 in the troposphere as well as in the stratosphere.

4. *Stratospheric H_2O*

The mass mixing ratio of H_2O in the stratosphere is about 3 ppm. It has been hypothesized that the equatorial tropopause temperature of about 195°K provides a cold trap for the H_2O being transported into the stratosphere. It is believed that this equatorial cold trap is the cause for the extreme dryness of the stratosphere. This cold trap hypothesis raises the possibility of a feedback between perturbations in O_3, CO_2, and stratospheric H_2O; i.e., perturbing O_3 or CO_2 would alter the tropopause temperature, which in turn may alter the stratospheric H_2O [*Chamberlain*, 1977; *Ramanathan et al.*, 1976]. As was suggested by Chamberlain, altering the stratospheric H_2O would modify the H_2O long-wave opacity, and the H_2O opacity modification could then modify the initial perturbations in T_s and the tropopause temperatures. Hence it is useful to estimate the sensitivity of T_s to changes in stratospheric H_2O concentrations.

Increasing (or decreasing) stratospheric H_2O would result in an increase (or decrease) in T_s primarily due to the increase (or decrease) in opacity of the pure rotation bands of H_2O. *Manabe and Wetherald* [1967] estimate that T_s will increase by 2°K for a fivefold increase in H_2O from the present-day value of 3 ppm, and *Wang et al.* [1976] estimate an increase of 0.65°K for a doubling of stratospheric H_2O.

5. *Minor Trace Species*

In addition to aerosols we have considered so far the effect of the three major trace species, H_2O, CO_2, and O_3, on the energy budget of the earth-atmosphere system. There are several other optically active minor trace species in the atmosphere whose importance to the global energy budget has only recently been realized. Table 9 lists the minor species (whose effects on long-wave radiation have been considered so far), the source for their presence in the atmosphere, the long-wave bands, and their possible effect on T_s from assumed modifications in their atmospheric concentrations.

Of the various species listed in Table 9 the fluorocarbons (CF_2Cl_2 and $CFCl_3$) and N_2O effects on T_s are of particular importance, because it is estimated that the atmospheric concentrations of these species may increase substantially because of anthropogenic sources.

The fluorocarbons are used as refrigerants and as propellants in aerosol cans. It has been estimated that by the end of the next century, if the present level of use is continued, the concentrations of these compounds in the atmosphere can increase by an order of magnitude from the present-day value of about 0.2–0.3 ppb (by volume) [*National Academy of Sciences*, 1976]. The primary reason for this expected buildup is the lack of any significant removal mechanisms in the troposphere. It is seen from Table 9 that at 2 ppb, fluorocarbons can have an appreciable effect on the climate. There are two reasons why fluorocarbons at exceedingly low concentrations (~1 ppb) have an appreciable effect on T_s. (1) Their bands are located in the 8- to 12-μm region (the so-called atmospheric window region), where the atmosphere is relatively transparent. Because of this relative transparency the atmospheric and surface temperatures are most sensitive to constituents that have absorption bands in the 8- to 12-μm spectral region. (2) The fluorocarbon bands are extremely strong. For example, the band intensities of the γ_8 and γ_4 bands are significantly larger (by a factor of 4) than the intensity of the 15-μm band of CO_2.

The use of fertilizers provides the primary source for the projected increase in N_2O. It has been suggested that the atmospheric concentration of N_2O may increase by as much as a factor of 2 by the year 2025 [*McElroy et al.*, 1977]. It is also speculated that the use of fertilizers may lead to an increase in

TABLE 9. Minor Trace Species and Their Effects on ΔT_s

Species	Major Present-Day Source in the Atmosphere	Band Center, μm	f_0, ppm (by volume)	δf_0	ΔT_s, °K R	ΔT_s, °K W
CF_2Cl_2	anthropogenic	9.13	1×10^{-4}	20		
		8.68				
		10.93				
$CFCl_3$	anthropogenic	9.22	1×10^{-4}	20	0.85	0.54
		11.82				
N_2O	natural	7.78	0.28	2		0.68
		14.0				
		4.5				
NH_3	natural	10.53	6×10^{-3}	2		0.12
HNO_3*	natural	5.9		2		0.08
		7.5				
		11.3				
		21.8				
CH_4	natural	7.66	1.6	2		0.28
CCl_4	natural and anthropogenic	12.99	1×10^{-4}	2	0.015	0.02
$CHCl_3$		13	1×10^{-4}	10	0.1	
		8.19				
CH_2Cl_2		14	1×10^{-4}	10	0.05	
		13.58				
		7.92				
CH_3Cl		13.66	1×10^{-4}	10	0.01	
		9.85				
		7.14				
SO_2	natural and anthropogenic	7.35	2×10^{-3}	2		0.03
		8.69				

Here f_0 is the assumed uniform tropospheric mixing ratio for the present-day atmosphere, and $\delta f_0 = f'/f_0$ is the assumed factor for increase in the mixing ratio, where f' is the mixing ratio in the perturbed atmosphere. Sources for the estimated value of ΔT_s are *Ramanathan* [1975*b*] (R) and *Wang et al.* [1976] (W). The ΔT_s results are for the FRH and FCT versions of the radiative-convective model.

* See *Wang et al.* [1976] for the altitude dependent profile.

NH_3 and HNO_3. *Wang et al.* [1976] raise the possibility that the CO released by combustion of fossil fuels may enhance the concentrations of CH_4 and CH_3Cl.

With the exception of N_2O and CH_4 the effects of the other minor species on ΔT_s scale linearly with respect to their concentrations. The absorption bands of these species are optically thin (for present concentrations), and consequently, the opacities (and ΔT_s) of these bands are linearly proportional to their concentrations. The results shown in the table have a broader implication for climate; i.e., trace species can have significant climatic effects even at exceedingly low concentrations if their long-wave bands are located in the 8- to 12-μm region.

H. Concluding Remarks

Here we will discuss the future use of radiative-convective models for climate studies. Such models should continue to be used for obtaining first estimates of the potential sensitivity of global surface temperature to perturbations in radiatively active gases for several reasons. First, the global surface temperature changes predicted by the model are in reasonable agreement with those obtained from the more complex three-dimensional general circulation models (GCM). For example, for a doubling of CO_2, *Manabe and Wetherald* [1967] obtained 2.24°K from a radiative-convective model, while they obtained 3°K from a GCM [*Manabe and Wetherald,* 1975]. It is important to note that both studies used the same radiation model. Second, because of its simplicity a radiative-convective model is capable of including many details of the radiative processes without overburdening the computer resources, and thereby it can give valuable information on the importance of such processes. Third, for climate change experiments, analysis of radiative-convective model results would be useful for GCM studies, since it is much more difficult to infer cause-effect relationships in a GCM model.

The important limitation of the model is that the model results are mostly of academic interest, since the model does not give any information about regional and latitudinal temperature changes. Furthermore, many of the model parameters (cloud amounts, surface albedo, relative humidity, and critical lapse rate, to name a few) are prescribed on the basis of present-day conditions which may not apply for large departures from present conditions. For example, the study by *Wetherald and Manabe* [1975] indicates that for a 2% increase in solar constant the radiative-convective model results for ΔT_s are within 20% of the GCM results, while for a 4% decrease in solar constant the two models differ by a factor of 2 in the estimated value of ΔT_s. Clearly, radiative-convective models cannot be applied for large perturbations from present conditions.

With respect to model improvements we offer the following suggestions. The ice albedo feedback can be included in the models relatively easily by making the surface reflectivity a function of T_s. *Wetherald and Manabe*'s [1975] or *Lian and Cess*'s [1977] results can be used for parameterizing surface reflectivity in terms of T_s. Inclusion of this coupling would improve the agreement with the GCM. Radiative-convective models underestimate ΔT_s, and the main reason is the neglect of ice albedo feedback in the model.

The next major improvement concerns the critical lapse rate. We showed that in the troposphere the value of 6.5°K/km is significantly different from the observed hemispheric mean lapse rate. This problem needs careful study, but a cursory examination of the observed hemispheric mean lapse

rate suggests that the following scheme of convective adjustment may be more appropriate than invoking a constant critical lapse rate. The critical lapse rate Γ_c should be equal to the moist lapse rate Γ_m when $\Gamma_m \leq 7°K/km$, and $\Gamma_c = 7°K/km$ when $\Gamma_m > 7°K/km$. The above scheme would simulate the transition from moist lapse rate in the lower troposphere to the constant lapse rate of 7°K/km within the middle and upper troposphere.

Undoubtedly more important than the above two improvements is the inclusion of cloud amount and cloud altitude feedback, but this must wait for better observational and theoretical studies that will indicate the nature of cloud feedback.

Acknowledgments. We thank J. W. Chamberlain for his encouragement to write this review and for his comments on the manuscript. We acknowledge R. E. Dickinson for bringing to our attention the important point that the critical lapse rate adopted in radiative-convective models is much larger than the observed global value. He also made several useful comments on the manuscript. We also thank S. B. Fels, W. C. Wang, and W. J. Wiscombe for their comments. We are grateful to H. Howard and E. Boettner for typing several versions of this lengthy manuscript. The National Center for Atmospheric Research is sponsored by the National Science Foundation.

REFERENCES

Ackerman, T. P., K. N. Liou, and C. B. Leovy, Infrared radiative transfer in polluted atmospheres, *J. Appl. Meteorol., 15,* 28–35, 1976. (Correction, *J. Appl. Meteorol., 16,* 1372–1373, 1977.)

Ambartsumyan, V. A., *Theoretical Astrophysics.* Pergamon, New York, 1958.

Armstrong, B. H., Analysis of the Curtis-Godson approximation and radiation transmission through inhomogeneous atmospheres, *J. Atmos. Sci., 25,* 312–322, 1968.

Augustsson, T., and V. Ramanathan, A radiative-convective model study of the CO_2-climate problem, *J. Atmos. Sci., 34,* 448–451, 1977.

Baes, C. F., H. E. Goeller, J. S. Olson, and R. M. Rotty, The global carbon dioxide problem, *Rep. ORNL-5194,* Oak Ridge Nat. Lab., Oak Ridge, Tenn., 1976.

Cess, R. D., The thermal structure within the stratosphere of Venus and Mars, *Icarus, 17,* 561–569, 1972.

Cess, R. D., A band absorptance formulation for Doppler broadening, *J. Quant. Spectrosc. Radiat. Transfer, 13,* 781–786, 1973.

Cess, R. D., Radiative transfer due to atmospheric water vapor: Global considerations of the earth's energy balance, *J. Quant. Spectrosc. Radiat. Transfer, 14,* 861–871, 1974.

Cess, R. D., Climate change: An appraisal of atmospheric feedback mechanisms employing zonal climatology, *J. Atmos. Sci., 33,* 1831–1843, 1976.

Cess, R. D., and S. C. Chen, The influence of ethane and acetylene upon the thermal structure of the Jovian atmosphere, *Icarus, 26,* 444–450, 1975.

Cess, R. D., and S. Khetan, Radiative transfer within the atmospheres of the major planets, *J. Quant. Spectrosc. Radiat. Transfer, 13,* 995–1009, 1973.

Cess, R. D., and V. Ramanathan, Radiative transfer in the atmosphere of Mars and that of Venus above the cloud deck, *J. Quant. Spectrosc. Radiat. Transfer, 12,* 933–945, 1972.

Chamberlain, J. W., A mechanism for inducing climatic variations through the stratosphere: Screening of cosmic rays by solar and terrestrial magnetic fields, *J. Atmos. Sci., 34,* 737–743, 1977.

Chandrasekhar, S., *An Introduction in the Study of Stellar Structure,* Dover, New York, 1957.

Chandrasekhar, S., *Radiative Transfer,* Dover, New York, 1960.

Chýlek, P., and J. A. Coakley, Jr., Aerosols and climate, *Science, 183,* 75–77, 1974.

Coakley, J. A., Jr., An efficient numerical approach to radiative-convective equilibrium, *J. Atmos. Sci., 34,* 1402–1407, 1977*a*.

Coakley, J. A., Jr., Feedbacks in vertical-column energy balance models, *J. Atmos. Sci., 34,* 465–470, 1977*b*.

Coakley, J. A., Jr., and G. W. Grams, Relative influence of visible and infrared optical properties of a stratospheric aerosol layer on the global climate, *J. Appl. Meteorol., 15,* 679–691, 1976.

Crutzen, P. J., SST's: A threat to the earth's ozone shield, *Ambio, 1,* 41–51, 1972.

Curtis, A. R., The computation of radiative heating rates in the atmosphere, *Proc. Roy. Soc., Ser. A, 236,* 156–159, 1956.

Deardorff, J. W., and G. E. Willis, The free convection temperature profile, *Quart. J. Roy. Meteorol. Soc., 93,* 166–175, 1967.

Dickinson, R. E., Infrared radiative heating and cooling in the Venusian mesosphere, 1, Global mean radiative equilibrium, *J. Atmos. Sci., 29,* 1551–1556, 1972.

Dickinson, R. E., Method of parameterization for infrared cooling between altitudes of 30 and 70 km, *J. Geophys. Res., 78,* 4451–4457, 1973.

Drayson, S. R., Atmospheric transmission in the CO_2 bands between 12 μm and 18 μm, *Appl. Opt., 5,* 385–391, 1966.

Drayson, S. R., Calculation of longwave radiative transfer in planetary atmospheres, Ph.D. thesis, *Rep. 07584-1-T,* 170 pp., Coll. of Eng., Univ. of Mich., Ann Arbor, 1967.

Drayson, S. R., and C. Young, The frequencies and intensities of carbon dioxide absorption lines beteween 12 and 18 microns, *Tech. Rep. 08183-1-T,* High Altitude Eng. Lab., Univ. of Mich., Ann Arbor, 1967.

Duncan, C. H., et al., Rocket calibration of the Nimbus 6 solar constant measurements, *Appl. Opt., 16,* 2690–2697, 1977.

Dyer, A. J., The flux gradient relation for turbulent heat transfer in the lower atmosphere, *Quart. J. Roy. Meteorol. Soc., 91,* 151–157, 1965.

Edwards, D. K., and W. A. Menard, Comparison of models for correlation of total band absorption, *Appl. Opt., 3,* 621–625, 1964.

Eliassen, A., and E. Kleinschmidt, *Dynamic Meteorology, Handb. der Phys.,* vol. XLVIII, 154 pp., Springer, New York, 1957.

Ellis, J. S., Cloudiness: The planetary radiation budget and climate, Ph.D. thesis, Dep. of Atmos. Sci., Colo. State Univ., Fort Collins, 1977.

Fels, S. B., and M. D. Schwarzkopf, The simplified exchange approximation: A new method for radiative transfer calculations, *J. Atmos. Sci.,* 1475–1488, 1975.

Fiocco, G., G. Grams, and A. Mugnai, Energy exchange and temperature of aerosols in the earth's atmosphere (0–60 km), *J. Atmos. Sci., 33,* 2415–2424, 1976.

Gierasch, P. J., Dissipation in atmospheres: The thermal structure of the Martian lower atmosphere with and without viscous dissipation, *J. Atmos. Sci., 28,* 315–324, 1971.

Gierasch, P. J., and R. Goody, A study of the thermal and dynamical structure of the Martian lower atmosphere, *Planet. Space Sci., 16,* 615–646, 1968.

Goody, R. M., *Atmospheric Radiation,* vol. I, *Theoretical Basis, Oxford Monogr. on Meteorol.,* Oxford at the Clarendon Press, London, 1964*a*.

Goody, R. M., The transmission of radiation through an inhomogeneous atmosphere, *J. Atmos. Sci., 21,* 575–581, 1964*b*.

Hansen, J. E., and L. D. Travis, Light scattering in planetary atmospheres, *Space Sci. Rev., 16,* 527–610, 1974.

Hansen, J. E., W. C. Wang, and A. A. Lacis, Mt. Agung eruption provides test of a global climate perturbation, *Science, 199,* 1065–1068, 1978.

Harshvardhan, and R. D. Cess, Stratospheric aerosols: Effect upon atmospheric temperature and global climate, *Tellus, 28,* 1–10, 1976.

Johnston, H. S., Reduction of stratospheric ozone by nitrogen oxide catalysts from SST exhaust, *Science, 173,* 517–522, 1971.

Krueger, A. J., and R. A. Minzner, A mid-latitude ozone model for the 1976 U.S. Standard Atmosphere, *J. Geophys. Res., 81,* 4477–4481, 1976.

Kuhn, W. R., and J. London, Infrared radiative cooling in the middle atmosphere (30–110 km), *J. Atmos. Sci., 26,* 189–204, 1969.

Kuriyan, J. G., Z. Shippony, and S. K. Mitra, Transmission function for infrared radiative transfer in an inhomogeneous atmosphere, *Quart. J. Roy. Meteorol. Soc., 103,* 511–517, 1977.

Lacis, A. A., and J. E. Hansen, A parameterization for the absorption of solar radiation in the earth's atmosphere, *J. Atmos. Sci., 31,* 118–133, 1974.

Leovy, C., Radiative equilibrium of the mesosphere, *J. Atmos. Sci., 21,* 238–248, 1964.

Lian, M. S., and R. D. Cess, Energy-balance climate models: A reappraisal of ice-albedo feedback, *J. Atmos. Sci., 34,* 1058–1062, 1977.

London, J., A study of the atmospheric heat balance, final report, contract AF19(122)-165, 99 pp., Coll. of Eng., N. Y. Univ., New York, 1956.

Manabe, S., Estimates of future changes of climate due to increase of

carbon dioxide concentration in the air, in *Man's Impact on Climate*, edited by W. H. Matthews, W. W. Kellogg, and G. D. Robinson, MIT Press, Cambridge, Mass., 1971.

Manabe, S., and B. G. Hunt, Experiments with a stratospheric general circulation model, 1, Radiative and dynamical aspects, *Mon. Weather Rev., 96*, 477–502, 1968.

Manabe, S., and R. F. Strickler, Thermal equilibrium of the atmosphere with a convective adjustment, *J. Atmos. Sci., 21*, 361–385, 1964.

Manabe, S., and R. T. Wetherald, Thermal equilibrium of the atmosphere with a given distribution of relative humidity, *J. Atmos. Sci., 24*, 241–259, 1967.

Manabe, S., and R. T. Wetherald, The effects of doubling the CO_2 concentration on the climate of a general circulation model, *J. Atmos. Sci., 32*, 3–15, 1975.

McElroy, M. B., S. C. Wofsy, and Y. L. Yung, The nitrogen cycle: Perturbations due to man and their impact on atmospheric NO_2 and O_3, *Phil. Trans. Roy. Soc. London, Ser. B, 277*, 159–185, 1977.

Murgatroyd, R. J., and R. M. Goody, Sources and sinks of radiative energy from 30 to 90 km, *Quart. J. Roy. Meteorol. Soc., 84*, 225–234, 1958.

National Academy of Sciences, Halocarbons: Effects on stratospheric ozone, report, Washington, D. C., 1976.

Newell, R. E., The global circulation of atmospheric pollutants, *Sci. Amer., 224*, 32–42, 1971.

Newell, R. E., and B. Weare, Factors governing tropospheric mean temperature, *Science, 194*, 1413–1414, 1976.

Oort, A. H., and M. Rasmusson, Atmospheric circulation statistics, *NOAA Prof. Pap. 5*, U.S. Dep. of Commer., Washington, D. C 1971.

Pollack, J. B., et al., Volcanic explosions and climatic change: A theoretical assessment, *J. Geophys. Res., 81*, 1071–1083, 1976.

Prabhakara, C., and G. Dalu, Remote sensing of the surface emissivity at 9 μm over the globe, *J. Geophys. Res., 81*, 3719–3724, 1976.

Priestley, C. H. B., *Turbulent Transfer in the Lower Atmosphere*, University of Chicago Press, Chicago, Ill., 1959.

Ramanathan, V., A study of the sensitivity of radiative-convective models, in *Second Conference on Atmospheric Radiation*, pp. 124–125, American Meteorological Society, Boston, Mass., 1975*a*.

Ramanathan, V., Greenhouse effect due to chlorofluorocarbons: Climatic implications, *Science, 190*, 50–52, 1975*b*.

Ramanathan, V., Radiative transfer within the earth's troposphere and stratosphere: A simplified radiative-convective model, *J. Atmos. Sci., 33*, 1330–1346, 1976.

Ramanathan, V., L. B. Callis, and R. E. Boughner, Sensitivity of surface temperature and atmospheric temperature to perturbations in the stratospheric concentration of ozone and nitrogen dioxide, *J. Atmos. Sci., 33*, 1092–1112, 1976.

Rasool, S. I., and S. H. Schneider, Atmospheric carbon dioxide and aerosols: Effects of large increases on global climate, *Science, 173*, 138–141, 1971.

Reck, R. A., Influence of surface albedo on the change in the atmospheric radiation balance due to aerosols, *Atmos. Environ., 8*, 823–833, 1974*a*.

Reck, R. A., Aerosols in the atmosphere: Calculation of the critical absorption/backscatter ratio, *Science, 186*, 1034–1036, 1974*b*.

Reck, R. A., Influence of aerosol cloud height on the change in the atmospheric radiation balance due to aerosols, *Atmos. Environ., 9*, 89–99, 1975.

Rodgers, C. D., The use of emissivity in atmospheric radiation calculations, *Quart. J. Roy. Meteorol. Soc., 93*, 43–54, 1967.

Rodgers, C. D., Some extensions and applications of the new random model for molecular band transmission, *Quart. J. Roy. Meteorol. Soc., 94*, 99–102, 1968.

Rodgers, C. D., Approximate methods of calculating transmission by bands of spectral lines, *Tech. Note 11G+1A*, Nat. Center for Atmos. Res., Boulder, Colo., 1976.

Rodgers, C. D., and C. D. Walshaw, The computation of infrared cooling rate in planetary atmosphere, *Quart. J. Roy. Meteorol. Soc., 92*, 67–92, 1966.

Sasamori, T., J. London, and D. V. Hoyt, Radiation budget of the southern hemisphere, *Meteorol. Monogr., 13*, 9–23, 1972.

Schneider, S. H., Cloudiness as a global climatic feedback mechanism: The effects on the radiation balance and surface temperature variations in cloudiness, *J. Atmos. Sci., 29*, 1413–1422, 1972.

Schneider, S. H., On the carbon dioxide-climate confusion, *J. Atmos. Sci., 32*, 2060–2066, 1975.

Schneider, S. H., and R. E. Dickinson, Climate modeling, *Rev. Geophys. Space Phys., 12*, 447–493, 1974.

Sellers, W. D., *Physical Climatology*, University of Chicago Press, Chicago, Ill., 1965.

Spiegel, E. A., Convection in stars, I, Basic Boussinesq convection, *Annu. Rev. Astron. Astrophys., 9*, 323–352, 1971.

Stone, H. M., and S. Manabe, Comparison among various numerical models designed for computing infrared cooling, *Mon. Weather Rev., 96*, 735–741, 1968.

Trafton, L. M., Model atmospheres of the major planets, *Astrophys. J., 147*, 765–781, 1967.

Vonder Haar, T. H., and V. E. Suomi, Measurements of the earth's radiation budget from satellites during a five-year period, *J. Atmos. Sci., 28*, 305–314, 1971.

Wallace, L., M. Prather, and M. J. S. Belton, The thermal structure of the atmosphere of Jupiter, *Astrophys. J., 193*, 481–486, 1974.

Walshaw, C. D., and C. D. Rodgers, The effect of the Curtis-Godson approximation on the accuracy of radiative heating rate calculations, *Quart. J. Roy. Meteorol. Soc., 89*, 122–130, 1963.

Wang, W. C., and G. A. Domoto, The radiative effect of aerosols in the earth's atmosphere, *J. Appl. Meteorol., 13*, 521–534, 1974.

Wang, W. C., et al., Greenhouse effects due to man-made perturbations of trace gases, *Science, 194*, 685–690, 1976.

Weare, B. C., and F. M. Snell, A diffuse thin cloud structure as a feedback mechanism in global climate modeling, *J. Atmos. Sci., 31*, 1725–1734, 1974.

Wetherald, R. T., and S. Manabe, The effects of changing the solar constant on the climate of a general circulation model, *J. Atmos. Sci., 32*, 2044–2059, 1975.

Wiscombe, W. J., and J. W. Evans, Exponential sumfitting of radiative transmission functions, *J. Comput. Phys., 24*, 416–444, 1977.

(Received February 14, 1978;
accepted May 11, 1978.)